AN IMPROVED ALGORITHM FOR PHASE-BASED VOLTAGE DIP CLASSIFICATION

Student Name: MOGAMAD SHAHEED JATTIEM
Student No: JTTMOG002

Supervisor: PROFESSOR K. FOLLEY

Thesis presented for the degree of Masters of Science in the Department of Electrical Engineering, University of Cape Town

I declare that I know the meaning of plagiarism and that all the work in this document save for that which is properly acknowledged, is my own.

Signature :……..….. Date: …….

ACKNOWLEDGEMENT

In the name of ALLAH, the most Beneficient, the most Merciful
All praise and thanks are due to ALLAH (Exalted is HE) for teaching mankind that which he knew not

I dedicate this work to my spiritual mentor, Shaykh Muhammad Nazim Al-Haqqani (Cyprus) – a true knower of the secret of electricity.

I also wish to thank my wife, Oemayma, for her unending support and motivation.

This work would not have been possible without the technical assistance of the following individuals: Assoc. Pr K Folly (UCT), Mr C Wosniak, (UCT), Dr M Schilder (Eskom), Mr HS Mostert (Eskom) and Pr P Pillay (Clarkson University, USA / UCT)

ABSTRACT

The growing global awareness of electrical power quality has led to an increase in voltage dip (sag) research. Within the study of voltage dips, methods of dip classification are an area of active research. Conventional methods of dip classification are based solely on the duration of the dip and the magnitude of the voltage deviation during the dip. This approach does not give insight into the phase behaviour during the dip or the type of fault which caused the dip.

To overcome the shortcomings of conventional dip classification methods, Dr M Bollen proposed a phase-based classification method having seven dip types (types A to G) in 1993. In addition, he developed two phase-based classification algorithms. The evaluation of the Bollen algorithm revealed that the Symmetrical Component method gives incorrect results in the event of phase shift while the Six-Phase algorithm fails if the angle of the reference voltage is set to 0°. The phase shift limitation is critical, since phase shift does occur in practice although more commonly on distribution cable networks.

In this thesis, a new phase-based algorithm is developed, which overcomes the shortcomings of the Bollen algorithms. The new algorithm computes the dip type based on the difference in phase angle between the measured voltages.

In software simulations, the new algorithm is able to distinguish between single phase and phase-phase dip types over the full range of phase shift and dip magnitude. To verify the new classification algorithm, dips are simulated in the laboratory and then classified using the new algorithm. The new algorithm was also evaluated by applying it to dips recorded on the Eskom Distribution network in the Western Cape.

The classification of voltage dips presents a challenge in terms of equipment performance and statistical behaviour of power networks. From this perspective, it is easy to accept that there cannot be a single classification method that applies equally well in all fields.

TABLE OF CONTENTS

CHAPTER ONE

INTRODUCTION TO VOLTAGE DIPS

1.1 BACKGROUND

The past three decades have seen a rapid increase in the global use of electrical loads which create voltage disturbances. Power electronic devices, fluorescent lighting, PC's and electronic loads are common examples of these. These loads draw non-sinusoidal currents from the supply network thereby distorting the network voltage which is supplied to other consumers. As a result, there has been an increased awareness of the quality of electricity. According to the Electric Power Research Institute (EPRI), 20% of the total electrical load in the USA was electronic in 1985. This was expected to jump to 50-60% by 2000 [33].

The increased use of devices which distort the supply voltage has also co-incided with an increase in the sensitivity of industrial equipment to voltage disturbances. Variable Speed Drives (vsd's) and Programmable Logic Controllers (PLC's) are examples of industrial equipment which are commonly affected by voltage anomalies, such as voltage dips, surges, voltage unbalance, etc.

1.2 POWER QUALITY PARAMETERS

The term "Power Quality" is used to describe the characteristics of the electrical product supplied by power utilities [39]. The characteristic parameters used to describe power quality are generally focused on the supplied voltage. These parameters are classified as illustrated below:

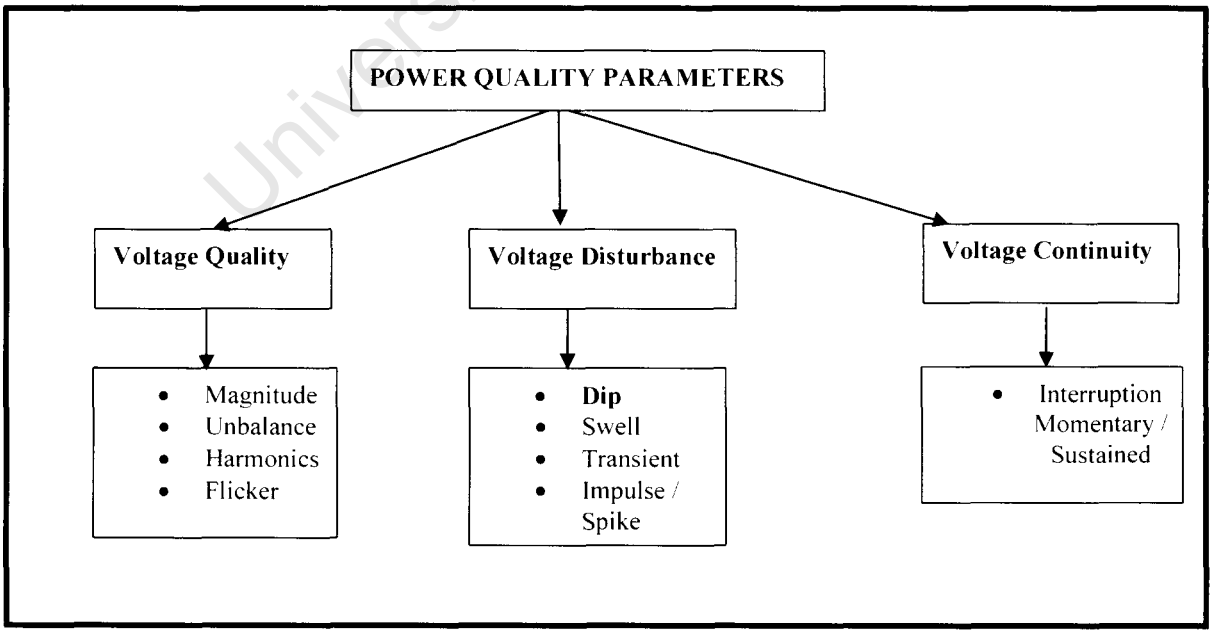

Fig 1.1 Classification of power quality parameters (*Adapted from [39]*)

In fig.1.1, the Voltage Quality parameters refer to the steady state voltage anomalies, such as unbalance, flicker, harmonics and voltage magnitude.
The Voltage Disturbance category refers to the transient voltage disturbances, such as dips (sags), surges and surge impulses.
The last category, Voltage Continuity, refers to the long term availability of supply

In the context of the Power Quality parameters in Fig.1.1, this research is focused on the voltage disturbance parameter called "dips".

1.3 VOLTAGE DIPS (SAGS)

1.3.1 Definition of dips

In North American countries, dips are referred to as "sags". Voltage dips are defined differently by international standards bodies, such as the IEEE and IEC.
Fig.1.2 illustrates the three phase sinusoidal voltages during a three-phase dip.

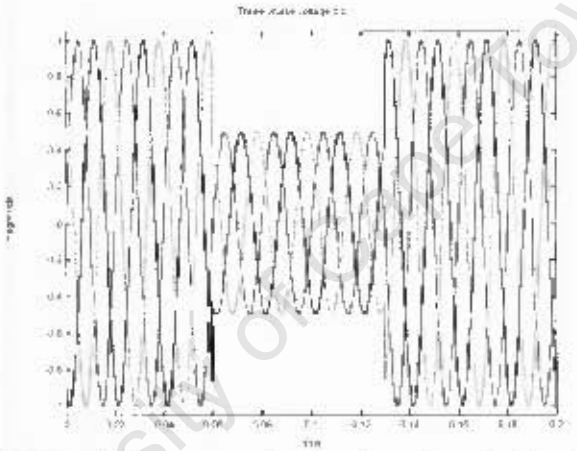

Fig.1.2 Sinusoidal representation of a three phase dip *(from [35])*

The IEEE Std. 1159 defines a dip (sag) as follows [35]

> *" 3.1.51 sag : A decrease to between 0.1 and 0.9 p.u. in rms voltage or current at the power frequency for durations of 0.5 cycle to 1 min.*
> *Typical values are 0.1 to 0.9 p u.*
> *NOTE To give a numerical value to a sag, the recommended usage is "a sag to 20%," of which means that the line voltage is reduced down to 20% of the normal value, not reduced by 20%. Using the preposition "of" (as in "a sag of 20%,"or implied by "a 20% dip") is deprecated."*

The IEC 61000-2-8 gives the following definition [35]

> *"2.1 voltage dip, voltage sag a sudden reduction of the voltage at a particular point on an electricity supply system below a specified dip threshold followed by its recovery after a brief interval"*

In South Africa, the National Rationalised User document NRS048-2:2004 is the standard dealing with power quality. It defines a voltage dip as follows:

"Sudden reduction in the r.m.s. voltage, for a period of between 20 ms and 3 s, of any or all of the phase voltages of a single-phase or a polyphase supply. The duration of a voltage dip is the time measured from the moment the r.m.s. voltage drops below 0,9 per unit of declared voltage to when the voltage rises above 0,9 per unit of declared voltage"

Should the voltage reduction last for longer than 3 seconds, the event would be categorised as either a momentary or a sustained interruption. In all the definitions presented above, it should be noted that the dip is denoted by a reduction in voltage (or current) magnitude below a specified threshold value over a duration of time.

Voltage dips are the most frequently occurring power quality phenomenon seen by consumers. Below are the results of a survey which studied the power quality at 24 Bell Labs computer installations, distributed geographically throughout USA. Measurements were taken over 270 months [9].

TABLE 1.1 SURVEY RESULTS FOR FREQUENCY OF VOLTAGE DISTURBANCES– *adapted from [9]*

DISTURBANCE	OCCURRENCE PERCENT
Voltage dips	87%
Impulses	7%
Power interruptions	5%
Overvoltages	1%

Source: Goldstein and Speranza "The Quality of US Commercial AC Power INTELEC, International Telecommunications Energy Conference, Washington D.C. 1982

In light of the above, it can be inferred that dips have the largest impact on consumers due to their high frequency of occurrence and the associated cost implication.

1.3.2 Causes of dips

The majority of dips are caused by events which occur frequently on electrical networks such as:

- Transmission line faults and associated protection operations
- Insulator flashovers and lightning
- Sudden load changes - such as motor starting, load shifting and transformer energisation
- Equipment failure
- Animal contacts (birds) and vandalism

Overhead lines are more common in rural distribution networks. As such, they are more prone to dips caused by line contacts and outside interference. In urban areas most of the distribution networks are underground. In this case, dips occur less frequently and are generally due to load effects such as motor starting and transformer energizing.

1.3.3 Propagation of dips

The effects of voltage dips are generally more apparent at the consumer from whom the dip originates. In South Africa it is estimated that about 60% of dip problems originate within customer installations [9].

However, dips also propagate through the electricity network and can affect neighbouring consumers. The extent to which the dip impacts on neighbouring consumers depends on:

- The system fault level
- The vector configuration of interposing transformers and
- The impedance of the electrical network

Therefore, the dips measured at a particular site will include dips which originate from the utility network, from neighbouring consumers as well as from within the measurement site itself.

1.3.4 Effects of dips

The common effects of voltage dips are:

- Visible 'dipping' of incandescent lights
- High Intensity Discharge lighting switches off for a dip and automatically restrikes after approximately 10 minutes.
- Tripping of variable speed drives (vsd) and other voltage-sensitive equipment
- Maloperation or failure of control circuitry, including motor contactors

Where such equipment forms part of a serial process, a dip can cause the entire process to be interrupted, often resulting in severe financial consequences to the consumer. As a consequence, claims for compensation are often lodged against the supply authority.
Industrial processes which depend heavily on the continuity of serial processes or whose processes are subject to short time-constants are particularly at risk due to voltage dips. Typical examples of such industries are extrusion plants, spinning plants, the pulp and paper industry, cement kilns and chemical plants. The figure below illustrates the results of research done to establish the cost of dips to a paper plant in South Africa [21].

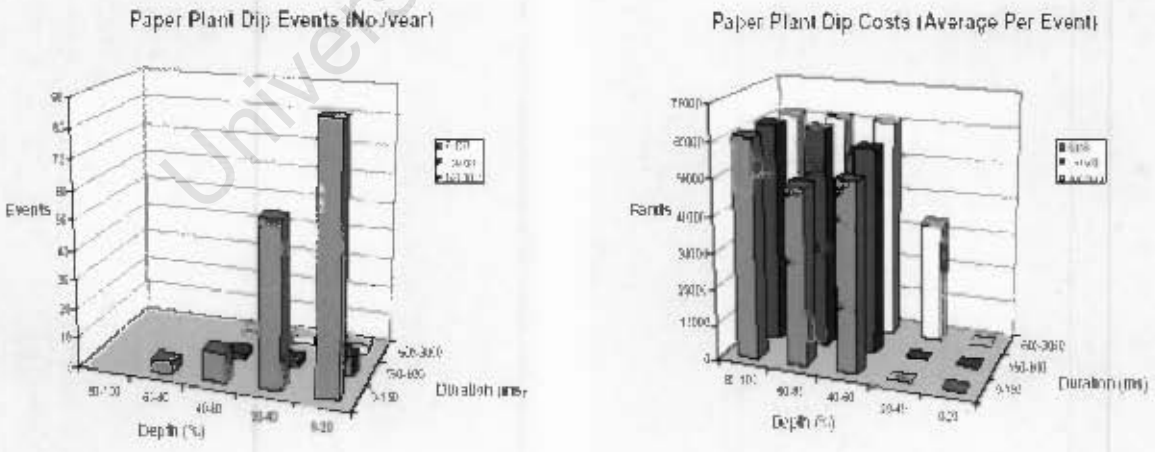

Fig.1.3 No. of voltage dip events (left) and the cost per event (right) for a typical paper plant *(extracted from [21])*

Fig.1.3 indicates the financial impact of voltage dips experienced at a typical paper plant. In this instance, the average cost per dip ranges between R50 000 to R60 000. In the semiconductor manufacturing industry, a dip could easily cause losses up to $1M [1].

Table 1.2 lists the typical impact of dips on some common industries.

TABLE 1.2 – THE IMPACT OF DIPS ON VARIOUS INDUSTRIES [adapted from 35]

Industry	**Impact**
Paper industry	Paper web has poor quality or breakdown.
Textile industry	Fabric defects or line is broken.
Steel industry	Wire extrusion winders can disturb the lining of the metal.
Newspaper press	Breakage/tearing of paper line
Petrochemical industry.	Contaminated tanks, pipes and restproducts
Chemical industry	Destroyed batch because disturbance in control, pumps, valves, autoclaves
Semiconductor industry	Destroyed chips, restart of testing of chips.

1.3.5 Mitigation of dips

The extent to which dip mitigation is implemented is a function of the costs involved and the importance of the process being protected.
Some of the important considerations for dip mitigation are listed below:

- Type of supply network (overhead or underground)
- Origins and causes of dips
- Earthing and wiring practices at customer installation
- Customer process sensitivity and equipment immunity

Due to the varying nature of the above factors, dip mitigation strategies are specific to each individual installation.

Some of the commercially available technologies for dip mitigation are listed in [9] as:

- Motor Generator Sets
- Uninterruptible Power Supply (UPS) Systems
- Superconducting Storage Devices
- Statordyne™
- Written Pole Motors

Cheaper mitigation alternatives are also available, such as [9]:

- Changing protection settings to limit the duration of dips
- Slugging of contactors to increase inertia
- Tapping up of supply transformers
- Tree trimming or installing anti-bird devices

1.4 POWER QUALITY REGULATION IN SOUTH AFRICA

The definition and classification of dips play an important role in the following aspects related to power quality:

- Dip Statistics and estimation
- Equipment Tolerance specifications
- Identification of dip causes
- Dip Mitigation strategies

In 1996, The South African National Electricity Regulator (NER) was charged with the regulation of power quality. The NRS048 standard was developed specifically for power quality. It initially includes specific limits for voltage dips which may be experienced by electricity consumers. The inclusion of dip limits resulted from the input of industrial interest groups who were concerned about the impact of dips on production processes and the possible deterioration of dip levels. The dip limits were based on dips being defined by voltage deviation and dip duration.

The role players involved in power quality are:

- electricity suppliers (licensees)
- consumers of electricity
- equipment suppliers
- regulatory bodies

Natural competition in a deregulated electricity supply industry is expected to lead to an improvement in levels of power quality. This point has however not yet been reached in South Africa. It is thus necessary to have guidelines for acceptable power quality as part of the license requirements for electricity suppliers [21].
In 2002, the NER published a document entitled "NER Directive on Power Quality" [21]. This document is aimed at managing power quality by outlining the roles and responsibilities of the role-players. This is in contrast to the initial regulatory approach which was based on adherence to specific dip limits. The NER chose to change its focus to the management processes itself by providing a general framework for managing the non-technical aspects of power quality.

Of particular interest to this research, is the responsibility placed on equipment suppliers in this document, wherein it states [21], p.45:

> *"Suppliers should be in a position to provide technical performance data for all power quality parameters. This performance data may be for basic and enhanced equipment specifications, and imply differentiated pricing."*

For suppliers to provide technical performance detail on dips, the dip immunity of equipment should be known and quantifiable. This in turn implies that equipment should be tested for dip performance and that suitable test protocols be available.

1.5 SPECIFYING EQUIPMENT IMMUNITY TO DIPS

The free movement of electrical equipment between countries and economies has resulted in the need for comparative analysis of dip tolerance specifications. Conformance to specified power quality limits is sometimes used as a criterion for certification. The

European Union (EU) uses compliance with its EMC standards, as a legal prerequisite for selling of electrical goods between its member countries.

With reference to voltage dips, it is important that equipment suppliers are able to specify the dip tolerance of their equipment. In [31] the dip tolerance of AC contactors was researched by performing dip tolerance tests. It was shown that existing dip definitions, which only use magnitude and duration, do not adequately describe the dip response of certain types of ac contactors.
It is shown that there is a noticeable change in dip tolerance with changes in the phase angle shift of a dip. The figure below is an extract from [31] which illustrates this point.

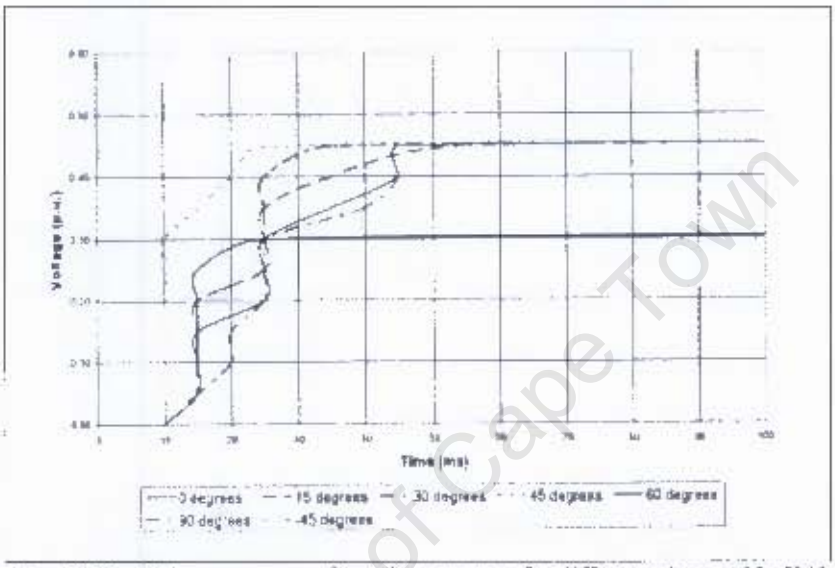

Fig. 1.4 Dip Tolerance curves for AC contactors for different phase shifts [31]

The tolerance curves in Fig 1.4 are interpreted as follows:
The x- and y-axes represent the dip duration and residual voltage magnitude respectively. The plotted curves represent the immunity of the contactor for different values of phase shift occurring during the dip.
If the contactor experiences dips with magnitude and duration values which lie above or to the left of a curve, the contactor will be able to withstand the dip without malfunctioning. For values below or to the right of a curve, the contactor drops out. The different curves clearly indicate that the dip tolerance changes for different phase shift values.

The limitation of the current dip classification methodology is also apparent when one considers the impact of phase shift on power electronic equipment which depends on zero-crossings for proper switching.

This important point is further substantiated by Sannino (et al) in [43], where the dip testing of voltage source converters is presented. The conclusion reached is that the dip immunity testing protocol for converters should include the response of the equipment to phase shift.

1.5.1 International Dip Immunity standards

Voltage dip immunity standards have developed globally from the need to specify dip performance in certain industries.
The major dip tolerance specifications in use are listed below:

1.5.1.1 Semiconductor Industry Equipment Immunity Curve: SEMI F47
This standard was developed in the USA specifically for the semiconductor industry. Due to the inherent dip sensitivity of the manufacturing processes involved, a specific dip tolerance curve was devised as a benchmark for semiconductor manufacturing equipment. For most immunity standards, the compliance is used as a quality criterion, which improves the marketability of the complying equipment.

1.5.1.2 ITIC (CBEMA)
Originally known as the CBEMA curve, this standard was originally developed in the 1970's to describe the tolerance of mainframe computer equipment to dips [29]. Since no other tolerance curves existed at the time, this standard was informally adopted by other industries. It essentially describes a tolerance envelope for a single-phase LV load. In 1996, the curve was revised and named after its new council, the Information Technology Industry Council (ITIC)

1.5.1.3 IEC 61000-4-11: Immunity Testing
Whereas the other standards classify dip tolerance as either "pass" or "fail" this IEC standard specifies various classes of dip performance for equipment rated <16A.

In 2005, Sannino (et al), proposed an extension of the existing IEC 61000-4-11 dip testing protocol to include phase angle shift as a test parameter. Using Matlab / Simulink™ software simulations, they effectively demonstrated the effects of dips with phase angle shift on a voltage source converter [43].

1.5.1.4 Swedish Industry Dip Tolerance Curve
This tolerance curve was developed in conjunction with the pulp and paper industry and was published in 2004.

1.5.2 Dip Immunity Standards in South Africa

There are currently no dip immunity specifications in place in the South African supply industry. Following the guidelines for equipment immunity set out by the NER, progress has been made in developing a standard specifically for equipment used in South Africa. The groundwork of this development has taken into account the international experiences and recognises the shortcomings of existing immunity specifications. The NER Power Quality Advisory Committee is tasked with compiling immunity classes for use in the South African context. The resulting specifications will form part of the next NRS048 standard [29].

1.5.3 Limitations of existing immunity standards

With the exception of the ITIC tolerance curve, all of the above cases consider the dip tolerance with respect to the dip magnitude and duration of a three-phase symmetrical dip. The application of these curves to all types of equipment is thus limited since they do not

consider the equipment tolerance to changes in phase angle or the point on wave at which the dip initiates.
These factors are important when one considers the dip behaviour of power electronic devices such as line-commutated converters and dc drives.
The classification of dips plays an important role in the interpretation of immunity specifications and test protocols.

1.5.4 Shortcomings of dip classification methods

When considering dip immunity, magnitude and duration are insufficient to classify dips. Changes in the voltage phase angles and the point of dip initiation are also important. This is crucial when considering the dip response of vsd's and AC contactors.

An inadequate dip classification method can lead to anomalies in the application of dip tolerance specifications.
Consider the following example:
Using the conventional classification method (i.e. magnitude and duration), a dip due to a single phase fault in a resistance grounded system may have the same magnitude and duration as a three phase fault. However, customers who operate vsd's may be unaffected by the single phase faults while three phase faults could cause vsd's to trip.

In [14], Bollen describes the shortcomings of classical classification methods by considering the difference between dips originating from three different sources i.e. transmission line faults, distribution line faults and transformer energizing.

The limitations of the existing classification methods are listed as [14]:

- The three phase character of the system is not considered in the classification
- Equipment performance cannot be fully defined without considering phase shift
- There is no consideration of the transfer of dips through transformers
- Dips due to transformer energisation are classified with the same magnitude as rectangular dips.
- Harmonic distortion during transformer energizing is not considered.

1.6 PHASE-BASED DIP CLASSIFICATION

The method of dip classification used is relevant to the relationships between the various roleplayers in power quality, i.e. regulatory bodies, licensees, consumers and equipment suppliers.
Whereas the conventional (magnitude-and-duration) methods are suitable for statistical reporting between licensees and regulatory bodies, they are inadequate to describe equipment dip performance as may be required from an equipment supplier.

Bollen [20] proposed a phase-based dip classification method which distinguishes between three phase and unbalanced dips. He proposed seven dip types (A to G) which take into account the phase relationship between the three phases.
The next challenge was to develop an algorithm to automatically classify 'raw' measured waveforms into their respective dip types. Bollen evaluated two such algorithms, i.e. the 'Six-Phase Method" and the "Symmetrical Component Method" in [19] and identified the

limitations of each. The Bollen dip types and algorithms are discussed in greater detail in Chapter 2.

In South Africa, Schilder and Koch applied the Bollen algorithms to actual dips from the Eskom National QOS Database [18] and found an accuracy of 50-80% for certain dip types. The 20% inaccuracy occurred under conditions where phase shift occurs during the dip.

1.7 RESEARCH HYPOTHESIS

The previous sections have highlighted the need for a phase-based dip classification method and highlighted the shortcomings of the existing phase-based algorithms.

In this thesis, a new phase-based dip classification algorithm will be developed. This algorithm will classify dips into the correct Dip-type category (A-G), as defined by Dr M Bollen. A time domain signal processing algorithm shall be used to track the phase changes during a voltage dip.

1.7.1 Value of this research

Phase shift during dips is a frequent occurrence on actual networks [18], [29]. The existing phase-based classification algorithms give incorrect results when [19]:

- Phase shift occurs
- The three-phase voltage vectors are rotated to a reference angle of 0°

Unlike the existing phase-based classification methods, the new classification algorithm does not make use of a transformation matrix. The phase angle information is extracted directly from the dip voltages, using a signal processing algorithm.

1.7.2 Research Limitations

Due to time constraints, the scope of this research was limited to exclude the following aspects

- Point-on-wave parameter
  Conventional dip classification methods do not take into account the point-on-wave at which the dip occurs. The importance of this parameter to dip immunity specification is highlighted in [29]. The new algorithm proposed in this thesis does not take into account the point-on-wave parameter in its classification.

- Complex dips
  Actual dips do not always conform directly to the seven dip types proposed by Bollen [29]. Such dips have been identified in [18] from the National Eskom PQ Database. The classification of such dip types is not attempted in this research.

1.7.3 Outline of Thesis Report

This thesis is structured as follows:

- Chapter 2 - a detailed literature survey on the topic of dip classification is presented, focusing on the research work done by Dr M. Bollen.
- Chapter 3 - The concepts and mathematical aspects related to dip definitions.
- Chapter 4 - The development of the new classification algorithm.
- Chapter 5 - A comparison (using MATLAB™ software) between the new algorithm and existing phase-based classification methods.
- Chapter 6 - A laboratory experiment is used to verify the performance of the classification algorithm.
- Chapter 7 - The application of the new algorithm to actual dip measurements taken on the Eskom Distribution network is presented.
- Chapter 8 - The final chapter consolidates the research findings and draws conclusions.

CHAPTER TWO

A LITERATURE STUDY ON DIP CLASSIFICATION

The term "dip classification" has ambiguous meanings in research literature. In some instances it is used to refer to the discrimination between various causes of dips [16].
In the context of this thesis, dip classification implies relating the behaviour of the voltage vectors during a dip to one of the pre-defined phase-based dip types.

To assess the use of phase-based dip definitions, different methods of presenting dip information are also studied. Lastly, the application of Digital Signal Processing tools and methods to the analysis of dips is investigated.

2.1 DIP PRESENTATION METHODS

In order to assess the use of phase-based dip definitions, the conventional methods of presenting dip information were reviewed.

The table below compares the most common methods of presenting dip information as identified by Andersson and Nillsen in [35].

TABLE 2.1: DIP PRESENTATION METHODS *(Adapted from [35])*

No.	Method of presentation	Advantage	Disadvantage
1	Voltage vs. duration plots – the lowest RMS phase value is plotted against the longest duration	Shows all voltage dips at a site on one chart	No Phase information or point on wave information
2	Contour chart - proposed by IEEE Std 1346, uses contour lines to represent the number of dips	Can be used to predict the number of events per year	No Phase information or point on wave information
3	SARFI(x) – System Average RMS Variation Frequency Index – provides information on the average voltage drop in a single phase.	Shows the number of dips as a % below a threshold (x)	No phase or point-on-wave information is included
4	The Sag Score – defined by the company Detroit Edison in power quality contracts	Relates the magnitude of the dip to its occurrence	Only considers magnitude and not duration or phase and point on wave information
5	UNIPEDE (IEC 61000-2-8) – a	Each entry presents	No information on

	table which shows for a specific site the number of voltage dips with magnitude and duration; RMS based on the worst phase	an average number of voltage dips with different severity	phase behaviour or point on wave
6	ESKOM Voltage Dip Table - Based on local standard NRS048 – 2:1996 (revised in 2004)	Presents an overview of dip performance and can be used to compare different sites	No information on phase behaviour or point-on-wave parameter
7	Loss of energy method – a relatively new method which compares the loss of energy to any predefined immunity curve	Can be used to describe how different equipment react to voltage dips	Does not consider magnitude, duration or unbalance.
8	Plot of 3-phase voltage vs. time	Considers magnitude, duration, and phase information for all three phases.	Only looks at a single dip, one cannot do comparison easily. Also requires lot of data storage
9	RMS-voltages and phase-angle versus time plot for representation	Same as above	Only shows one dip at a time
10	Symmetrical components - the three components are used in three contour plots.	Relates to the characterisation of unbalanced dips	No information on phase behaviour or point-on-wave

Most of the conventional methods of presenting dip information are based on the magnitude and duration of the dip. These methods are generally used for presenting statistical dip information and to enable dip prediction.

The plotting of sinusoidal voltage behaviour during against time is advantageous from a phase behaviour perspective, but it only looks at a single dip event at a time and is not the best option for statistical dip studies. This method can be used to analyse the nature of the fault which caused the dip.

The presentation methods which include phase information (8, 9 and 10 above) do not reference the dip to any predefined dip-type.
It can be concluded that different methods of dip presentation exist, depending on the aspect of application.

2.2 PHASE-BASED DIP CLASSIFICATION AS PROPOSED BY DR M BOLLEN

One of the foremost researchers in dip classification is Dr M. H. J. Bollen. In this section, some of his contributions to the field of dip classification are reviewed.

2.2.1 Shortcomings of existing dip definitions

In 1993 Bollen highlighted the shortcomings of existing dip classification methods by considering the difference between rms voltage profiles of dips originating from three different sources i.e. transmission line faults, large motor starting and transformer energizing [14].
The limitations of the existing methods are listed as:

- The three phase character of the system is not considered in the classification
- There is no direct link with equipment performance
- No consideration of the transfer of dips through transformers
- Non-rectangular events are classified too severe
- Harmonic distortion during transformer energizing is not considered.

2.2.2 Bollens' dip types

After highlighting the limitations of the existing methods based on magnitude and duration, Bollen [20] proposed four dip (Type A to Type D) categories in 1997 based on the type of faults which cause the dip. Three additional types (E to G) were later added (in 2000) to cater for faults as experienced by different load connections (star or wye-). The phasor diagrams of the Bollen dip types are shown in Fig.2.1 below.

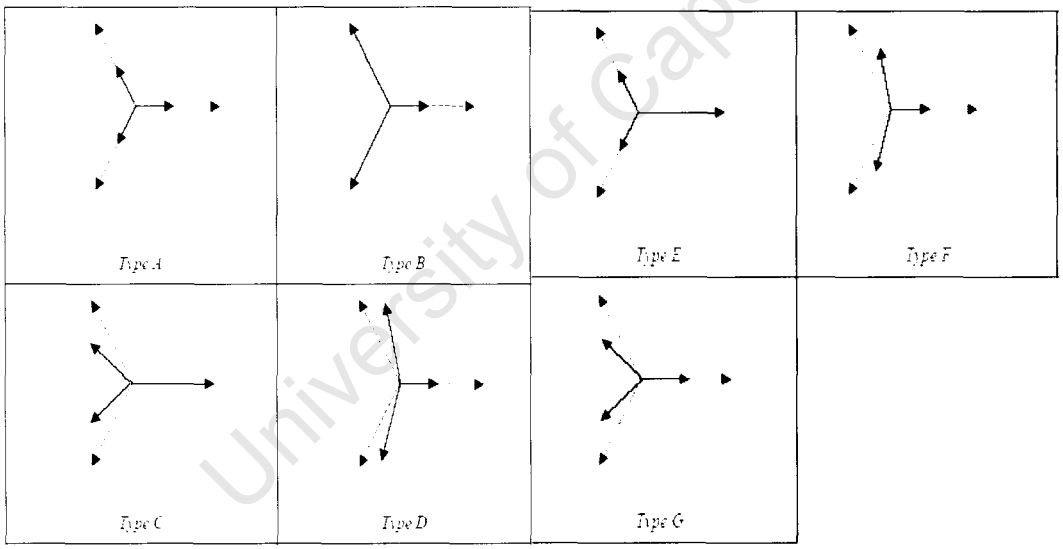

Fig. 2.1 Bollens' Phase-based Dip Types; before (dotted) and after (solid) dip

The seven dip types are arranged based on the number of phases with the most severe voltage drop [15].
Type A - This is due to a three-phase balanced fault and manifests as an equal reduction in the RMS value in all three phases. The phase angle relationships are unaffected.

Type C, E and G – Two retained voltages are much smaller than the third. These dips are caused by phase-phase faults.

Type B, D and F– One voltage drops more than the other two voltages. These dips are caused by phase-ground faults.

A subscript ($_{a, b}$ or $_{c}$) is used to provide information about the phases affected by the dip. In types B, D and F, the subscript denotes the faulted phase, whereas in types C, E and G, the subscript denotes the unaffected phase. The subscripted phase is called the symmetrical phase. For example, a type D_a dip would be caused by a phase-ground fault on the a-phase. In [20], Bollen applies symmetrical components to describe how the dip types are derived from the type of fault. He also describes, mathematically, the transformation of unbalanced dips through various transformer windings and the impact on star and delta connected loads.

Although seven distinct dip types were initially presented, Bollen showed that all seven types can basically be described as either three-phase, single phase or phase-phase dips, i.e. types A, C and D.

In [43], Sannino demonstrated the application of the new dip types to voltage tolerance testing. By showing the sensitivity of a self-commutated voltage converter to phase-shifted dips, they proposed an extension to the existing test protocol (IEC 61000-4-11).

2.3 BOLLENS' DIP CLASSIFICATION ALGORITHMS

After defining the phase-based dip types, a classification algorithm was required. In [19], Bollen describes two algorithms which attempt to classify measured dip voltages into one of three dip types, i.e. types A, C or D. These types correspond to three-phase, phase-phase and single-phase faults respectively.

Both algorithms make use of the sequence component transform to derive the positive and negative sequence voltages. In addition, two new complex quantities are introduced to quantify the dip, i.e.

- V - The characteristic voltage. The modulus and the argument of V are referred to as the magnitude and phase angle jump of the dip

- F - The PN Factor – it gives an indication of the unbalanced nature of the dip. The lower its value, the more balanced the dip is.

For an unbalanced dip, the individual phase voltages are functions of V and F.
For example, for a type C_a dip, as shown in Fig. 2.2 [19]

$$V_a = F$$

$$V_b = -\tfrac{1}{2} F - \tfrac{1}{2} j V\sqrt{3}$$

$$V_c = -\tfrac{1}{2} F + \tfrac{1}{2} j V \sqrt{3} \qquad (2.1)$$

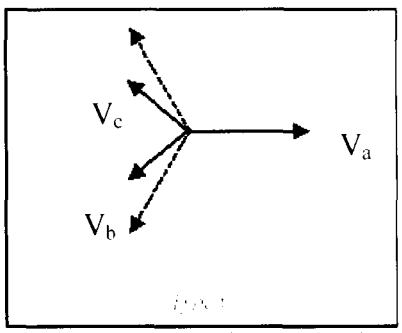

Fig. 2.2 Vector plot for Type C dip

Similarly, mathematical expressions are derived for the phase voltages in all the dip types in terms of the two complex parameters, V and F [19].

2.3.1 Symmetrical Component Algorithm

This algorithm transforms the measured voltages (V_a, V_b and V_c) into the positive and negative sequence voltages using Fortesque's transformation matrix.
The dip type is then directly related to a factor T, which is defined from the sequence components as shown below [19].

$$T = \frac{\arg\left(\frac{v2}{1-v1}\right)}{60°} \tag{2.2}$$

Where:

v1 is the positive sequence voltage
v2 is the negative sequence voltage

The dip is then classified depending on the rounded value of T, according to the following table [19].

TABLE 2.1 SYMMETRICAL COMPONENT METHOD

T (rounded value)	Dip Type
0	Ca
1	Dc
2	Cb
3	Da
4	Cc
5	Db

The initial formula for *T* in *(2.2)* gave erroneous results when the dip voltages were shifted due to the impact of the load. The equation was subsequently modified by introducing a constant of 20 degrees to compensate for the additional phase shift caused by the load [19].

$$T = \frac{\arg\left(\frac{v2}{1-v1}\right)}{60°} + 20° \tag{2.3}$$

From equation *(2.3)*, it is noted that this algorithm bases its result on the difference in phase between the positive and negative sequence components.

2.3.2 Six Phase Algorithm

In this algorithm the measured dip voltages are first transformed using the Sequence component transformation matrix. Thereafter, the zero sequence component is subtracted and the three voltages re-constructed. The algorithm then computes six RMS voltages,

namely, the three phase voltages (V_a, V_b and V_c) and the phase-phase voltages (V_{ab}, V_{bc} and V_{ac}) [19].

$$V_A = RMS\left\{v_a - \frac{1}{3}(v_a + v_b + v_c)\right\} \tag{2.4}$$

$$V_B = RMS\left\{v_b - \frac{1}{3}(v_a + v_b + v_c)\right\} \tag{2.5}$$

$$V_C = RMS\left\{v_c - \frac{1}{3}(v_a + v_b + v_c)\right\} \tag{2.6}$$

$$V_{AB} = RMS\left\{\frac{v_a - v_b}{\sqrt{3}}\right\} \tag{2.7}$$

$$V_{BC} = RMS\left\{\frac{v_b - v_c}{\sqrt{3}}\right\} \tag{2.8}$$

$$V_{CA} = RMS\left\{\frac{v_c - v_a}{\sqrt{3}}\right\} \tag{2.9}$$

The dip type is then determined by which of the six values are the lowest, as per the table below.

TABLE 2.2 SIX PHASE ALGORITHM CLASSIFICATION (*Adapted from [19]*)

LOWEST VOLTAGE	**DIP TYPE**
V_A	Da
V_B	Db
V_C	Dc
V_{AB}	Cc
V_{BC}	Ca
V_{AC}	Cb

The dip parameters (V and F) can be obtained directly from these six voltages whereby: The characteristic voltage (V) is the lowest of the six rms voltages and the PN factor is the highest of the six.

2.4. LIMITATIONS OF BOLLEN ALGORITHMS

To evaluate the phase-based algorithms, Bollen applied them to a number of simulated dips and to a measured dip [19]. The range of simulated dips was limited to single phase and phase to phase faults. This experiment concluded that the six-phase algorithm gives incorrect outputs for large phase-angle jumps.
The symmetrical component algorithm proves to be more accurate, except in cases where the PN factor (F) is less than unity. This can occur due to the effect of the load current on magnitude and phase shift of the dip voltages. This problem is alleviated by adding a constant of 20 degrees in the formula for T.

In South Africa, Schilder and Koch [18] evaluated both algorithms by applying them to measured dip data from the Eskom National QOS Database. Here too, it was found that some practically measured dips do not fit exactly into the seven dip types proposed by Bollen. The Bollen algorithms were able to classify only 50%-80% of dips correctly when the phase angle of one of the voltages was set to 0°.
The results also confirmed the inaccuracy of the six phase algorithm to large phase-angle jumps with an accuracy of 88 – 93%.

The dip survey done by Eskom in 2000 [29] provides important results for the application of the Bollen dip types to measured data. The measured data reveals that dips can exhibit phase shift behaviour which does not correspond to the Bollen dip types. It is seen that the seven dip types proposed by Bollen do not describe the full range of observed phase behaviour on actual networks.

2.5. DIP CLASSIFICATION FROM RMS VALUES

In 2004, Bollen (et al) proposed a method of dip type classification based on the measured RMS dip voltages [15]. This is in contrast to the previously developed algorithms [16] which require complex voltages. Most power quality instruments store only the rms values of the dip voltages. It would thus be valuable to classify dips based solely on the rms dip voltages. The algorithm proposed in [15] distinguishes between the dip types based on the relationship between the lowest and highest rms voltages during the dip. A summary of these relationships for the various dip types are shown below.

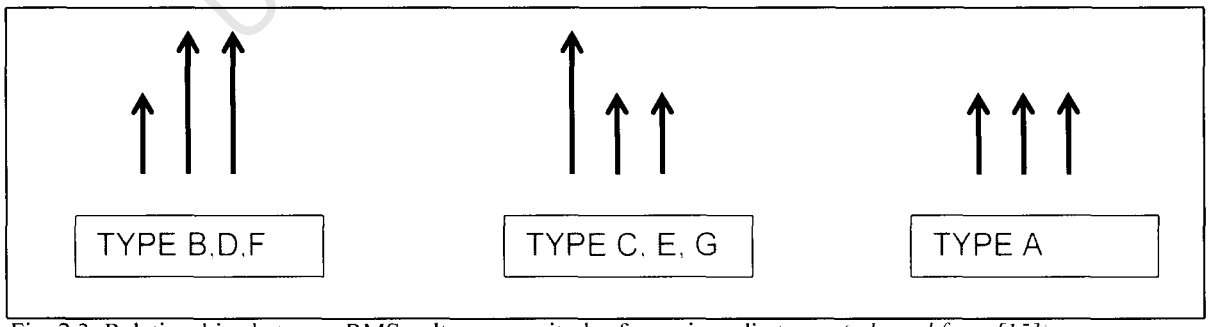

Fig. 2.3: Relationships between RMS voltage magnitudes for various dip types *(adapted from [15])*

By arranging the RMS voltages in ascending order, V_x, V_y and V_z are obtained, where V_x is the smallest RMS voltage and V_z is the highest RMS value.
Bollen then derives mathematical formulae to distinguish between the dip types based on these sorted values [15].

The limitation of this classification method is noted in that it gives incorrect results when large phase-angle shifts occur. It also requires that the zero-sequence impedance component be equal to the positive and negative sequence components; a condition which does not occur on HV networks [15].

2.6 AN ESKOM SURVEY OF PHASE ANGLE SHIFT ON LV NETWORKS

From the discussion thus far, it is deduced that the phase shift is an important factor in the correct classification of dips. In 2000, Eskom conducted a study to measure the phase shift behaviour of dips at an LV site in Kwazulu Natal [29]. 100 dips were recorded and classified based on the phase angle behaviour during the dip.
The following figure summarises the observed phase shift behaviour [29].

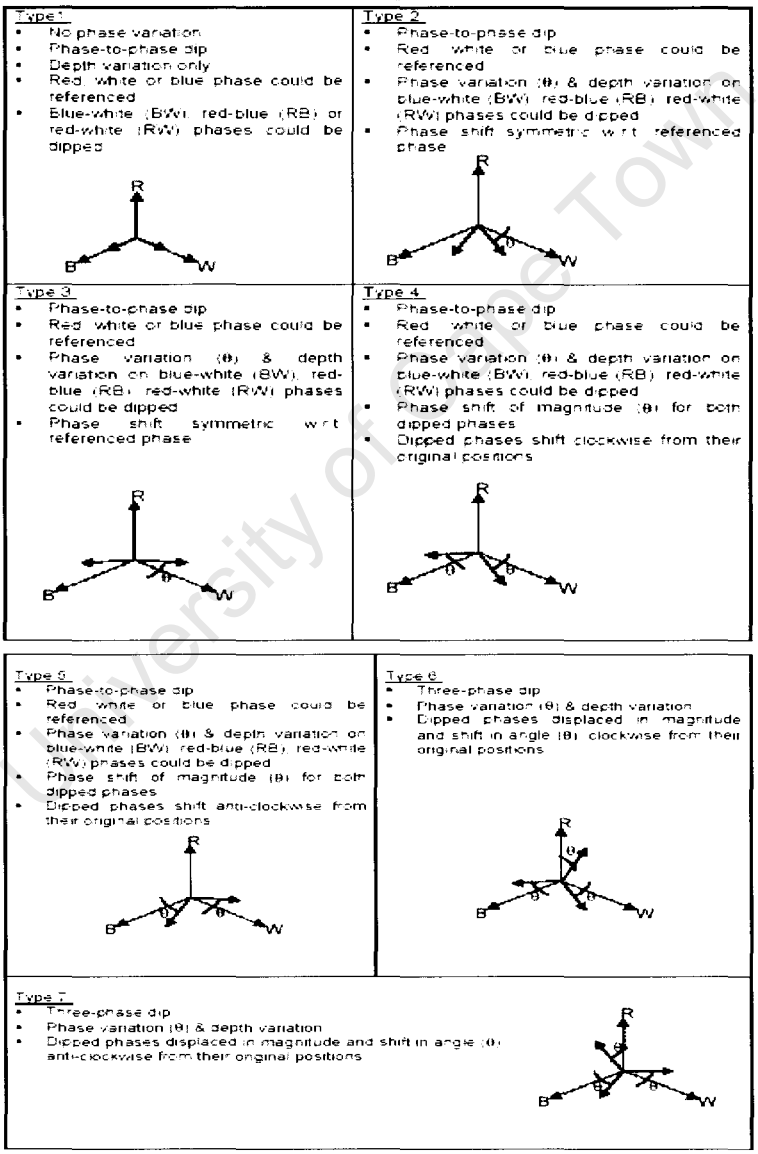

Fig. 2.4 Dip phase shift behaviour at an LV site - Eskom Survey *(taken from [29])*

2.7 DSP TOOLS AND METHODS USED IN POWER SYSTEMS

This section identifies various Digital Signal Processing (DSP) tools and methods used in power quality measurement and analysis. The objective of this section is to determine which tools or methods may be used in phase-based dip classification.

2.7.1 Sequence Component Transform

This mathematical transform is applied widely in the analysis of power systems and rotating machines. The Sequence Component Transform converts an unbalanced three-phase vector system into three separate, balanced vector systems, i.e. positive, negative and zero sequence systems. Analysis is easily performed on the sequence components and the result can be re-converted to the three-phase system.

The transformation equation is shown below [44]:

$$V_a = V_{0a} + V_{1a} + V_{2a}$$

$$V_b = V_{0b} + a^2 V_{1b} + a V_{2b}$$

$$V_c = V_{0c} + a V_{1c} + a^2 V_{2c} \qquad (2.10)$$

Where: $a = -\frac{1}{2} + j\sqrt{3}/2 = 1\angle 120$

V_a, V_b and V_c are the three-phase voltage vectors
(V_{1a}, V_{1b} and V_{1c}), (V_{2a}, V_{2b}, V_{2c}) and (V_{0a}, V_{0b}, V_{0c}) are the positive, negative and zero sequence components respectively

This tool is readily applied to the analysis of dip voltages. In section 2.3 of this chapter, it is shown how the sequence components of the dip voltages are used for phase-based dip classification.

2.7.2 The Fourier transform

One of the most popular tools used for the estimation of amplitudes and phase of signals is the Fast Fourier Transform (FFT). It effectively decomposes a time-domain signal into its constituent frequency components and is ideally suited to harmonics studies. The FFT is best applied to signals which are periodic in nature [42]. Its application is limited in that it does not present changes in the frequency components of a signal with respect to time.

This problem is overcome through the use of the Short Time Fourier Transform (STFT), which is a time-localized version of the FFT. In [42], Gu and Bollen compare the STFT with the Dyadic Wavelet for application to studying voltage disturbances. They conclude that the discrete STFT is generally more suitable.

In relation to dip classification, the Fourier transform tools can be used to estimate the magnitude of a dip, as well as for extracting the phase.

2.7.3 Wavelet Theory

A recently developed DSP tool is Wavelet Theory. It was first introduced in 1994 and has found widespread application in Power Systems [30]. The Wavelet Transform (WT) is a linear transformation, similar to the FFT. It also allows the identification of the frequency components of a given input signal to be localized in time. In [30], the specific areas of power systems research to which Wavelets have been applied are analysed. The table below compares these areas of application in terms of the relative percentage of available publications, as at June 2002

TABLE 2.3 THE APPLICATION OF WAVELETS IN POWER SYSTEMS *(adapted from [30]*

Research area	**% of available publications of wavelets in power systems**
Protection	36
Power Quality	32
Transients	11
Partial Discharges	4
Power measurements	2
Load Forecasting	3
Other	12

2.7.3.1 Wavelets in Power quality classification and dip identification

In the area of dips, wavelets have been applied successfully in conjunction with pattern recognition techniques for:

2.7.3.1.1 Discriminating between power quality parameters- differentiating between dips and other transient phenomenon such as swells, interruptions, harmonics, overvoltage and flicker. The following tools are applied in conjunction with wavelets:

- Rule-based expert systems [33]
- Inductive Inference algorithm using decision trees [38].
- Analysis of Probability Density Function [5] and [7].
- Neural networks [6].
- Fuzzy Reasoning [38]

2.7.3.1.2 Identification of dip origin - Identifying the event which caused the dip such as line faults, capacitor switching, motor starting or convertor operation

- Bayesian Method [16]

In none of the researched literature, has wavelets been used to extract the phase angle relationship between dip voltages, and as such it is not suited to phase-based dip classification.

2.7.4 The Ziarani / Konrad Algorithm

From the definitions of the dip types, it is deduced that magnitude and phase information are required to enable the classifications.

Phase-lock loops (PLL) and adaptive notch filters are popularly used in DSP applications to track the phase of signals [2].
A novel algorithm for extracting amplitude, phase and frequency directly from sinusoidal signals was developed by Ziarani and Konrad in [2]
The algorithm is governed by a set of non-linear differential equations which minimizes the error between the input signal and the approximated output.

The Ziarani algorithm has been applied successfully in numerous fields, such as biomedical studies, active vibration control and noise-rejection of sinusoidal signals [2]. This tool is ideally suited to be used in phase-based dip classification since it can provide the phase angle of the dip voltages. A thorough description of the Ziarani algorithm is given in Chapter 4.

2.8 SUMMARY

In this chapter the existing literature on dip classification and the presentation of dips has been reviewed.
Existing methods of presenting dip information were reviewed, which showed limited use of phase information when describing dips.

The dip-types presented by Bollen were introduced (type A to G) and the two symmetrical transform algorithms for dip classification were discussed.
An alternate method of dip classification based on RMS voltages was also reviewed. All of these classification methods have limitations when large phase-angle shift occurs.

A different type of phase-based classification, based on a survey done by Eskom was also presented. This classification was derived by considering the actual phase shift behavior of 100 voltage dips measured at an Eskom LV measurement site in Kwazulu Natal. This survey showed that practical measured dips do not always conform to the dip types proposed by Bollen.

A separate study in South Africa by Schilder and Koch [18] confirmed that the seven dip types cannot be applied to all dips. In addition, phase shifts of up to 127 degrees have been measured, indicating that the Bollen algorithms' sensitivity to phase shift is a significant limitation.

The application of various DSP tools and methods to dips was also looked at, with the objective of identifying suitable technologies for dip classification.

In comparison to the mathematical tools and methods mentioned in this chapter, the Ziarani / Konrad algorithm is preferred for dip classification since it readily provides the magnitude and phase information required for dip classification.

CHAPTER THREE

CONCEPTS OF PHASE-BASED DIP CLASSIFICATION

This chapter presents the mathematical theory associated with phase-based dip classification.

3.1 PHASE-ANGLE SHIFT DURING DIPS

One of the shortcomings of conventional dip classification methods is that the shift in phase angle associated with dips is not taken into account.

The phase shift is described by considering the voltage at the point of common coupling (PCC). The PCC refers to the nearest electrical point between the origin of a dip and the connection of other loads. This is demonstrated in Fig. 3.1 where the Substation Busbar is the PCC between the load and the fault [43].
The impact of a dip on adjacent consumers is taken from its measurement at the PCC.

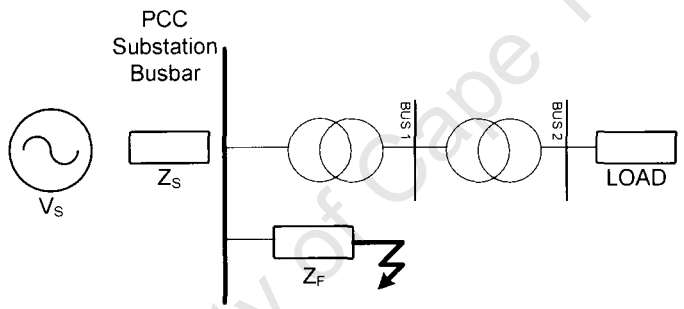

Fig.3.1 Illustration of PCC [43]

This phase-angle shift is attributed to two phenomena [31], i.e.

- The difference in the impedance angle (X/R ratio) between the source and a feeder. This leads to an initial phase shift (jump) at the PCC.
- In addition, the transformation of the dip from the PCC to the point of measurement through transformer windings causes an additional phase-angle shift.

Depending on the above factors, a phase-angle shift will occur between the pre-dip voltage and the during-dip voltage as seen at the point of measurement.

Phase angle changes can cause sensitive equipment to malfunction. In [20], Bollen highlights the negative impact of phase-angle changes to vsd's which depend on zero-point crossings for correct switching.

3.2 MATHEMATICAL DERIVATION OF PHASE SHIFT FOR GIVEN FEEDER IMPEDANCES

In the case of a three phase fault, the voltage at the PCC is given in [43] as:

$$V_{pcc} = V_{predip} \frac{Z_f}{Z_f + Z_s} \tag{3.2}$$

Where: V_{pcc} is the voltage at the PCC
V_{predip} is the pre-dip voltage
Z_f is the impedance between the PCC and the fault, and
Z_s is the source impedance

If there is a difference between the impedance angles of the source impedance and the feeder impedance, the phase angle of the voltage will experience a shift (jump) for the duration of the fault. The phase shift is the argument of V_{pcc} and is expressed as [43]:

$$\arg(V_{pcc}) = Tan^{-1}(\frac{Xf}{Rf}) - Tan^{-1}(\frac{Xf + Xs}{Rf + Rs}) \tag{3.3}$$

Where:
R_f is the real component of the impedance between the PCC and the fault
X_f is the reactive component of the impedance between the PCC and the fault
R_s is the real component of the source impedance
X_s is the reactive component of the source impedance

Where the impedance angles of Z_s and Z_f are similar, the phase shift is small. This is typically the case for high voltage transmission lines. In the case of distribution networks, a larger phase shift can be expected due to the high X/R ratio of distribution transformers combining with the overhead lines or cables having relatively lower X/R ratio.

In practice, relatively small phase shifts are experienced on transmission networks. Larger shifts up to 60 degree are predicted for cable networks. In Eskom networks, shifts of up to 127 ° have been measured [18].

3.3 MATHEMATICAL EXPRESSIONS FOR PHASE-BASED DIP TYPES

The Symmetrical Component Transform is the basis for the derivation of the phase-based dip types as discussed in Chapter 2. To quantify unbalanced dips, Bollen introduced two complex quantities, i.e. the characteristic voltage V, and the P-N factor F.

The vector forms of the voltages can be expressed in terms of the characteristic voltage, V as shown in Table 3.1

TABLE 3.1: VECTOR EXPRESSIONS FOR PHASE-BASED DIP TYPES (adapted from [43])

Type A $V_a = V$ $V_b = -\frac{1}{2}V - \frac{1}{2}jV\sqrt{3}$ $V_c = -\frac{1}{2}V + \frac{1}{2}jV\sqrt{3}$	**Type B** $V_a = V$ $V_b = -\frac{1}{2}V - \frac{1}{2}j\sqrt{3}$ $V_c = -\frac{1}{2}V + \frac{1}{2}j\sqrt{3}$
Type C $V_a = 1$ $V_b = -\frac{1}{2} - \frac{1}{2}jV\sqrt{3}$ $V_c = -\frac{1}{2} + \frac{1}{2}jV\sqrt{3}$	**Type D** $V_a = V$ $V_b = -\frac{1}{2}V - \frac{1}{2}j\sqrt{3}$ $V_c = -\frac{1}{2}V + \frac{1}{2}j\sqrt{3}$
Type E $V_a = 1$ $V_b = -\frac{1}{2}V - \frac{1}{2}jV\sqrt{3}$ $V_c = -\frac{1}{2}V + \frac{1}{2}jV\sqrt{3}$	**Type F** $V_a = V$ $V_b = -\frac{1}{2}V - j\left(\frac{1}{3} + \frac{1}{6}V\right)\sqrt{3}$ $V_c = -\frac{1}{2}V + j\left(\frac{1}{3} + \frac{1}{6}V\right)\sqrt{3}$
Type G $V_a = \frac{2}{3} + \frac{1}{3}V$ $V_b = -\left(\frac{1}{3} + \frac{1}{6}V\right) - \frac{1}{2}jV\sqrt{3}$ $V_c = -\left(\frac{1}{3} + \frac{1}{6}V\right) + \frac{1}{2}jV\sqrt{3}$	

V represents the Characteristic Voltage

3.4 PROPAGATION OF VOLTAGE DIPS

By virtue of dip propagation, measurements at a particular site could include dips which originate from the utility transmission network, from neighboring consumers as well as from within the measurement site itself.
The propagation of dips through transformer windings is accompanied by changes in the phases affected. The change in phase is due to the vector configuration of the transformer windings. This cause different dip types to be measured at different voltage levels for the same fault.
The voltage divider model is used in [43] to explain how the dip type changes, due to propagation through transformers with a Dy vector configuration.

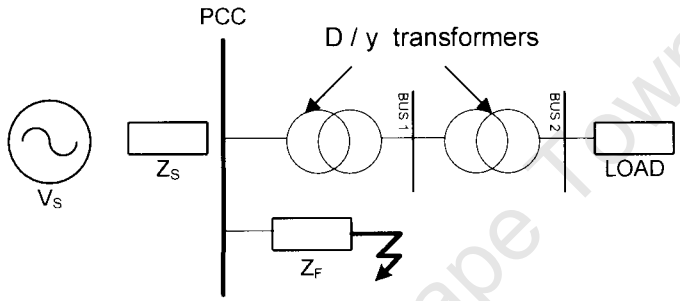

Fig.3.2 Changes in dip type due to transformer winding (from [43])

TABLE 3.2: DIP TRANSFORMATION DUE TO PROPAGATION [43]

Fault type	Dip at PCC	Dip at BUS 1	Dip at BUS 2
3-phase	A	A	A
Phase-ground	B	C*	D*
Phase-phase-ground	E	F	G
Phase-phase	C	D	C

Note: * indicates that the dip magnitude is not equal to dip magnitude at PCC

Table 3.2 demonstrates how the dip type changes between the primary and secondary side of the Dy transformer, depending on the fault type. This is important when trying to relate a dip to a fault which occurs at a different voltage level
Anderson and Nillson [35] also presents dip transformation effects for different transformer winding configurations. The table below combines the results presented by the two publications, i.e. [35] and [43].

TABLE 3.3 TRANSFORMATION EFFECTS FOR DIFFERENT TRANSFORMER WINDINGS [35] , [43]

Transformer winding configuration	Effect on dip-type transformation
YNyn,	the individual phases are unaffected
Dd, YNy, Dz, Yy, Yyn	The zero-sequence is removed
Dy, Yz, Yd	The phase voltage is changed to line voltage or vice versa

3.5 SUMMARY

In this chapter, it is shown that a mathematic model for voltage dips can be derived from elementary circuit theory by using the voltage-divider principle and Ohms Law. An expression for Phase Shift in terms of the source and fault impedances is presented.

The propagation of dips and the changes in phase angle through various transformer windings is also discussed. This provides insight to the identification of dips which occur remotely at different voltage levels.

CHAPTER FOUR

A NEW PHASE-BASED DIP CLASSIFICATION ALGORITHM

This chapter describes the development of a new dip classification algorithm and its implementation using Matlab™ and Simulink™ software.
The literature survey presented in Chapter 2 identified many algorithms which distinguish between power quality phenomena such as dips, surges and harmonics. In addition, much has been published on algorithms which classify dips based on the origin of the fault i.e. motor starting and capacitor switching. Some of the commonly used tools are neural networks, wavelet decompositions, Fuzzy Logic, Kalman Filtering and Bayesian method.

4.1 MOTIVATION FOR NEW ALGORITHM

A new phase-based classification algorithm was needed to overcome the shortcomings of the existing phase-based algorithms.

The new algorithm was necessitated by:

- The inaccuracy of the existing algorithms in the presence of phase shift
- The prevalence of phase shift in actual networks necessitated

The objective of the new algorithm was thus to develop a simple algorithm that would classify dips into the seven dip types described in Fig.2.1. In addition, the new algorithm should be robust with regards to phase shifts during the dip.

4.2 CONCEPT BEHIND NEW ALGORITHM

The new algorithm is based on the principle that each dip type can be uniquely described by a combination of the magnitude and phase relationships between the dip voltages. The algorithm aims to extract the magnitude and phase relationships directly from the measured dip voltages and to match these to the predefined characteristic of each dip type.

In [15], Bollen derived the magnitude relationships for the dip types. For a single phase fault, the voltage magnitude of the faulted phase will be low while the other two voltages will be greater in value and close together. For phase-phase faults, two phases are reduced and of similar magnitude while the third voltage is greater in magnitude. In the case of a three phase fault, all three voltages are reduced and of similar magnitude.
The new algorithm extracts the phase angle information directly from the sinusoidal voltages using the adaptive algorithm presented by Ziarani in [2]. The magnitude and phase descriptions of the dip are then compared to the known relationships for the seven dip types.

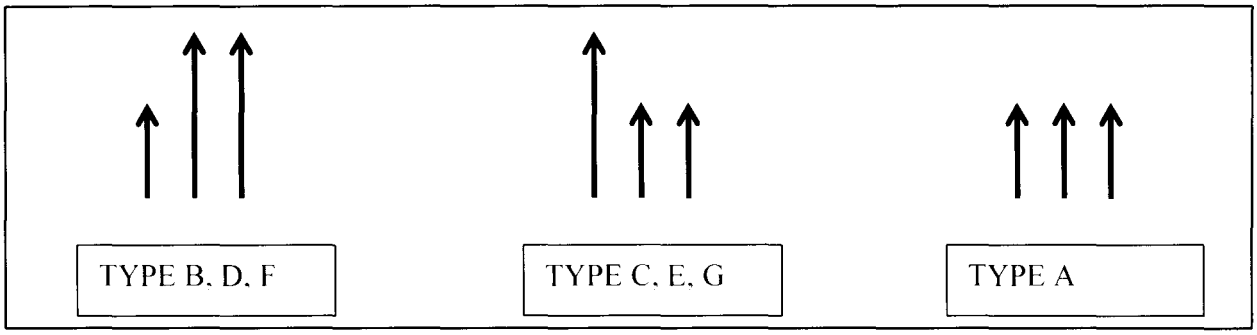

Fig. 4.1 Relationships between voltage magnitudes for various dip types

The magnitude relationships described in Fig.4.1 are coded into a decision table as shown below

TABLE 4.1 DECISION TABLE FOR MAGNITUDE RELATIONSHIPS

Dip Type	Magnitude relation
A	abs(Vz-(2*Vy)+Vx)<0.02*Vnom AND Vz < 0.9*Vnom
B	Vz-Vy < Vy-Vx AND Vz < 0.9*Vnom
C	Vz-Vy>Vy-Vx AND Vz < 0.9*Vnom
D	Vy>0.9*Vnom AND (Vz-Vy < Vy-Vx) AND (Vx<0.9*Vnom)
E	(Vz>0.9*Vnom) AND (Vz-Vy > Vy-Vx) AND (Vx<0.9*Vnom)
F	(Vz<0.9*Vnom) AND (Vz-Vy < Vy-Vx)
G	(Vz<0.9*Vnom) AND (Vz-Vy > Vy-Vx)

*Vx, Vy and Vz are the sorted voltages with Vz being the highest voltage. V_{nom} is the nominal voltage

In all of the above instances, the algorithm checks whether a dip has occurred by comparing the voltages to the dip threshold level, which is normally set at 90% of the nominal network voltage. The expression used to test for dip type A also checks that the voltages are close together.

4.3 OVERCOMING THE PROBLEM OF PHASE SHIFT

The existing phase-based algorithms introduced by Bollen (i.e. Symmetrical component algorithm and Six-phase algorithm) both produce incorrect results in the case of phase shift. The new algorithm attempts to overcome this limitation in the following manner:
For single phase faults (types B, D and F), the phase difference between the two unfaulted phases is used as a distinguishing criteria.
For phase-phase faults (types C, E and G), the phase difference between the faulted phases is used to determine the phase behaviour during the dip. This concept is illustrated in Fig.4.2 and Fig. 4.3

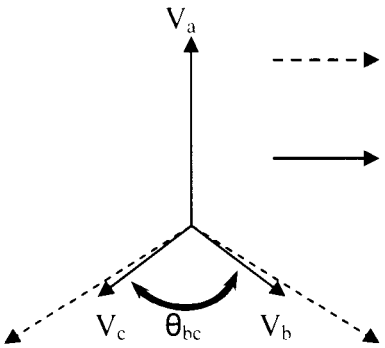

Fig. 4.2: Type Ca dip with minimum phase shift

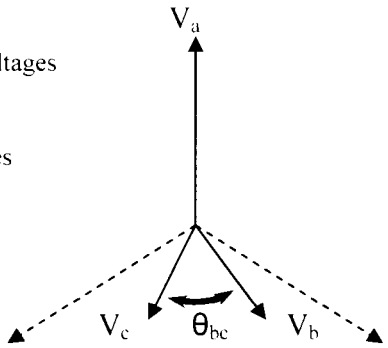

Fig. 4.3: Type Ca Dip with big phase shift

The two figures above depict a dip of the same type, with varying phase shift. If the Bollen symmetrical component algorithm is applied, the two vector sets will give different sequence components. If the amount of phase shift is big enough, the Bollen algorithm could give different answers for the same dip type due to the different sequence components.
However, if the angular difference (θ_{bc}) is used to distinguish this dip type, it can be seen that this value stays within the applicable range, i.e. <120°, despite the phase shift. In a similar manner, the angular phase difference is used to identify the other dip types. The table below lists the actual phase criteria used for each dip type.

TABLE 4.2 RELATIONSHIPS BETWEEN PHASE ANGLE DIFFERENCES FOR VARIOUS DIP TYPES

Dip type	Θ_{ab}	Θ_{bc}	Θ_{ac}
A	120	120	120
Ba	-	120	-
Bb	-	-	120
Bc	120	-	-
Ca	-	<120	-
Cb	-	-	<120
Cc	<120	-	-
Da	-	>120	-
Db	-	-	>120
Dc	>120	-	-
Ea	-	120	-
Eb	-	-	120
Ec	120	-	-
Fa	-	>120	-
Fb	-	-	>120
Fc	>120	-	-
Ga	-	<120	-
Gb	-	-	<120
Gc	<120	-	-

In the above table, the subscript in the dip type denotes the symmetrical phase.

It can be seen from Table 4.2 above that some of the dip types exhibit the same phase relationship. In particularly types D and F are similar and types G and C are similar. For

these dip types, the uniqueness is obtained from the magnitude relationships shown in Fig. 4.1. The algorithm uses the phase and magnitude identifiers mutually to determine the dip type.

4.4 SIMULINK™ IMPLEMENTATION OF THE NEW ALGORITHM

Matlab / Simulink™ was chosen as the software platform for the simulation and evaluation of the new algorithm. Fig. 4.4 shows the experimental setup used to simulate and test the new algorithm. The following sections describe the blocks mentioned in Fig. 4.4

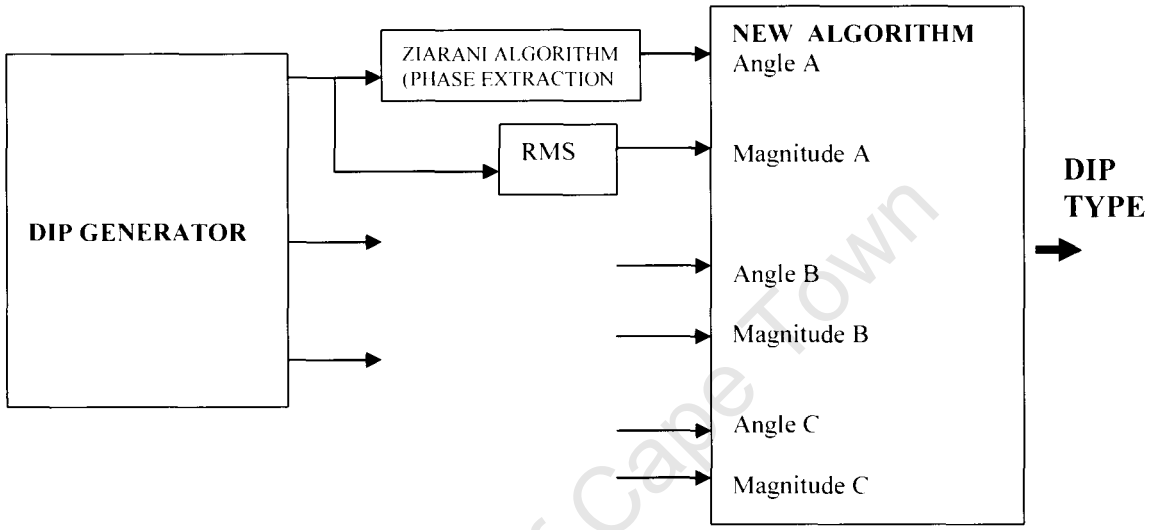

Fig. 4.4: Block diagram of software experimental setup

The "Dip Generator" block creates three phase sinusoidal dip waveforms. The Ziarani algorithm is then used to extract the phase while a RMS function is applied to the sinusoid waveforms to give the RMS magnitudes.
The classification algorithm has as its input, the phase angle and RMS input for each phase and produces the dip type as its output. The new algorithm is distinguished in that it does not transform the sinusoidal voltages to a distinct "analysis" plane such as the Fourier transform or Sequence Component transform. Instead, the phase angles of the sinusoids are used directly as inputs to the algorithm.

The detailed Simulink™ model of the experimental setup is included in Appendix B.

4.5 DIP GENERATOR MODEL

To test the classification of various dip types, it was required to simulate the dip behaviour of the three-phase sinusoidal voltages. This was done by creating a unique model using the available model blocks in the Matlab Simulink™ library. This model is called the Dip Generator. An illustration of the Simulink™ model for the Dip Generator is given in Appendix B-2.

This model simulates a dip by switching between a "healthy" sinusoid and a "dip" sinusoid, where the variables of phase and magnitude can be independently set for each sinusoid. The switching between the two sinusoids is determined by a level detection mechanism built into the switch. The switch is controlled by a programmable square waveform which

can be changed to give different durations and timings of dips. In this manner it is able to simulate dips of various:

- Pre- and post dip voltage
- Dip Duration
- Dip Magnitude
- Phase angle shift

The "healthy" sinusoids for the three phases have a phase difference of 120 degrees to represent the normal three-phase voltages.

In its current state, the Dip Generator Model is only able to simulate rectangular dips. Although actual dips may exhibit non-linear behaviour (e.g. Motor starting dips), a rectangular dip is considered sufficient for the purposes of testing the classification algorithms.

4.6 THE ZIARANI / KONRAD SINUSOID EXTRACTION ALGORITHM

In order to extract the phase angle behaviour associated with the dip from its sinusoidal representation, the method proposed by Ziarani and Konrad [2] was used. This extraction algorithm locks on to a sinusoidal component of its input signal and tracks its variations over time. Its dynamic behaviour is governed by a set of non-linear differential equations, which employ the methods of least squares error minimisation and the method of steepest descent [2]. The Simulink™ implementation of this algorithm is shown in Fig.4.6

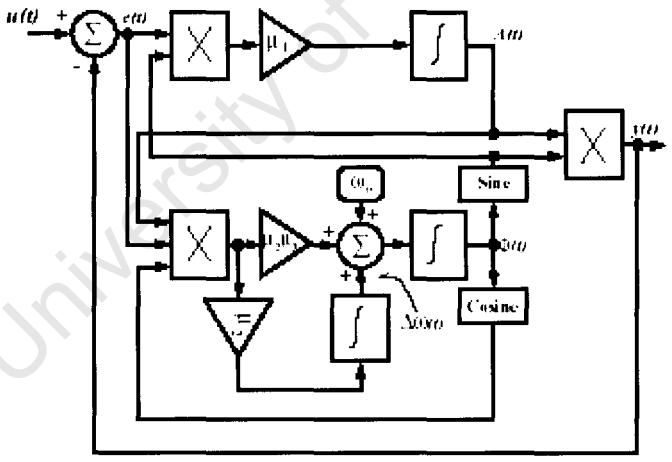

Fig. 4.5 Simulink™ Block Diagram of the Ziarani / Konrad Sinusoid extraction algorithm (from [2])

In Fig.4.6 μ_1, μ_2 and μ_3 are the tuning parameters for the extraction algorithm. These values can be adjusted to give a balance between the speed and accuracy of the algorithm. A formal methodology for tuning the μ parameters does not exist, and a process of trial and error is required to optimise the algorithm output.

A more detailed explanation of the development and characteristics of this algorithm is given in [2]. For the purposes of its application to the dip classification algorithm, it is sufficient to study the dynamic phase-tracking behaviour of the algorithm.

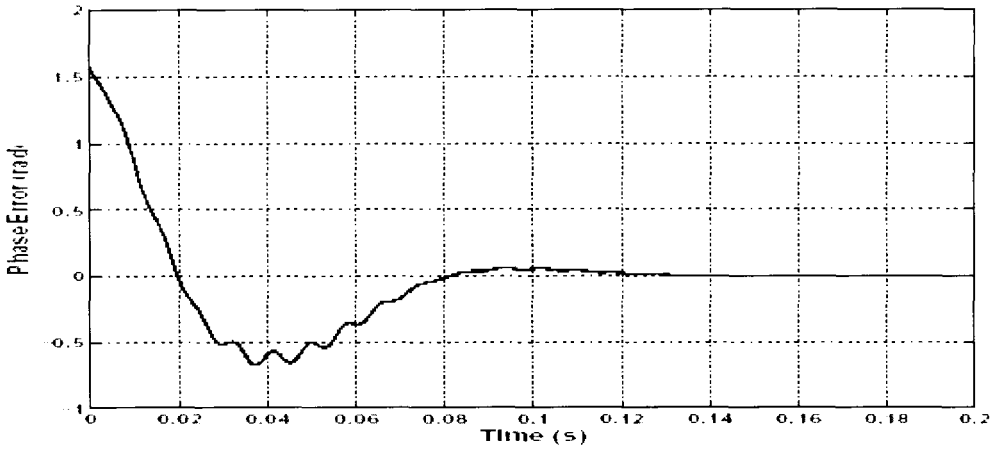

Fig. 4.6 Phase-tracking performance of Ziarani algorithm (from [2])

The above graph shows the phase-tracking performance of this algorithm in extracting the phase from an input signal. It is derived by applying a sinusoidal signal of constant phase angle and comparing the phase angle of the output waveform to this known value.
It can be seen that the algorithm requires about 100ms to lock on to the phase of the input signal. The speed of the algorithm can be adjusted by tuning the gain factors used in the model. Consequently, there is a trade-off with the accuracy of the approximation.

Since the input signal is a dip waveform, it is also relevant to study the response of the algorithm to changes in the magnitude of the input voltage. The graphs below show the response of the magnitude, frequency and phase of the output signal to a step change of 10% in the magnitude of the input waveform [2].

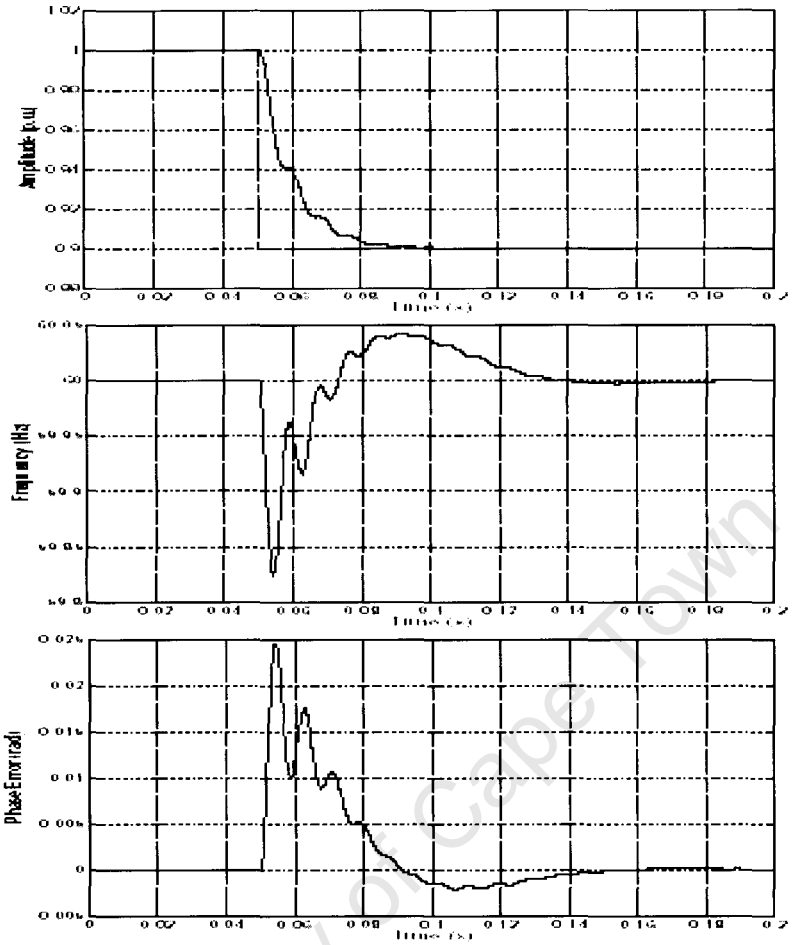

Fig.4.7 The response of the Ziarani / Konrad algorithm to a step change in Input voltage *(from [2])*

It can be seen that the algorithm can take up to 100ms to stabilise after the step change occurs. This has an impact on the output values for short dip events.

There are other signal processing methods which perform the same task. A comparative study of the Ziarani / Konrad algorithm and two other popular algorithms, i.e. Extended Kalman Filtering and the Method of Regalia, highlights the advantages of the Ziarani / Konrad algorithm in terms of noise immunity and robustness [2].

Although the algorithm is able to track the magnitude, frequency and phase of the fundamental component of the input signal, it is used only for extracting the phase angle of the input voltage.

4.7 MATLAB™ IMPLEMENTATION OF THE NEW CLASSIFICATION ALGORITHM

The new classification algorithm is modelled as a number of Matlab™ functions, listed below:

- The Show_Class function

- The Create_Dip_Vector Function
- The Match_dip function

A text printout of these functions in Matlab™ code is given in Appendix A.
The diagram which follows illustrates the structure of the classification algorithm and its functions.

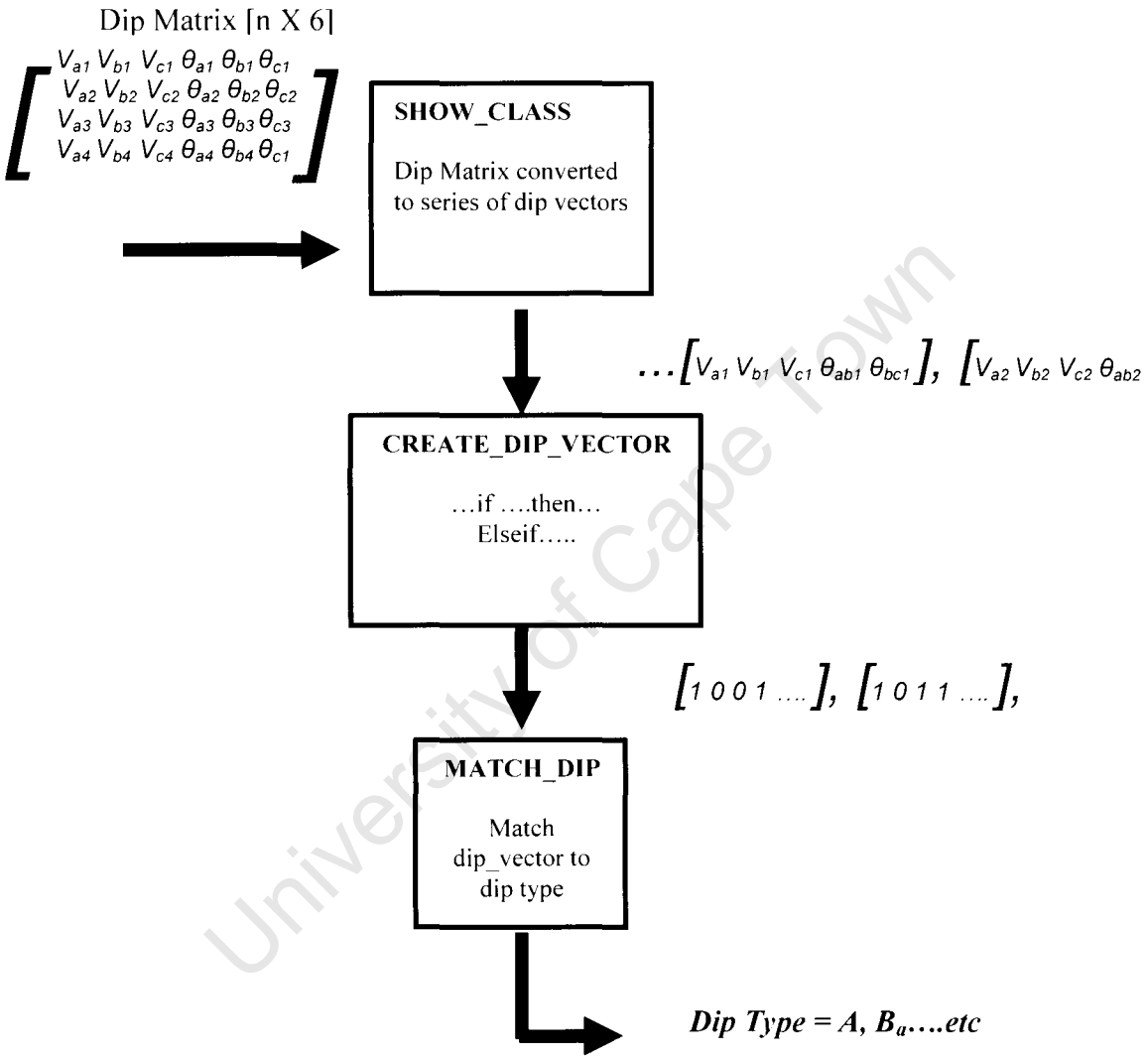

Fig.4.8 Block diagram of new classification algorithm using Matlab™ functions

Matlab™ is ideally structured to use matrices and vectors as a data type, hence the algorithms' functions are written to utilise these data types.
Using Matlab™, the measured dip voltages are transformed into a [n X 6] Dip Matrix. The following subsections describe how the new algorithms' functions produce a dip classification from the Dip Matrix.

4.7.1 The Show Class function

This function converts the dip matrix to a stream of 6-element vectors, where each vector represents a point of measurement.
This function then applies the classification function recursively so that a classification result is obtained for each dip "vector".

4.7.2 The Create Dip Vector function

This function performs the actual classification. It applies the decision –making criteria listed in Table 4.1 and Table 4.2 and attempts to match the input dip vector to the unique relational conditions of each dip type by using the logical AND operator until a match is found.
Programmatically, this is done using a unique combination of "If..then..else..statements" corresponding to each dip type. If the dip vector does not match any of the dip types, an error message is returned.
To identify the magnitude relationship of the input vector, the three voltage values are arranged in ascending order. The dip type is then based on the difference between the highest and lowest values, as shown in Fig.4.1
This is similar to the approach mentioned in [15], wherein Bollen derives mathematical expressions for the voltage relationships

Based on the conditions stipulated above, the input vector is matched to a corresponding dip type with each dip type being represented by a unique 5 bit binary vector.
This function decodes the dip type into a 5 bit binary number. For each classification event, there are nineteen possible dip types. An additional binary number is used to represent the case where the input vector does not match any of the known dip types. This gives a total of twenty distinct outputs whereas the total number of states that can be represented with 5 bits is 2^5 (32), there are thus twelve states which are not used.

4.7.3 The Match Dip Function

The task of this function is to decode the 5-bit dip vector into its corresponding text equivalent which is then presented as the output of the algorithm

4.8 FEATURES OF NEW ALGORITHM

Whereas the algorithms presented by M Bollen in [16] focus only on the analysis of the most popular dip types, i.e. type C and D, the new algorithm classifies all unbalanced dip types as well as symmetrical dips.
Of particular importance is the fact that the algorithm is robust with regard to phase jumps, since it considers the phase angle differences between the phases and not the actual phase values. This also makes it insensitive to the choice of reference for phase angle values. This is in contrast to the methods presented by Bollen; where the accuracy of the algorithm is dependant on the phase jump and the angle of the reference voltage [15].
An advantage of using the phase difference as an identifier, is that it allows the classification of some dips which do not fall directly into the Bollen dip classes. In [18],

Schilder and Koch found a number of practically measured dips which do not match the seven dip classes directly. An example of this is shown below.

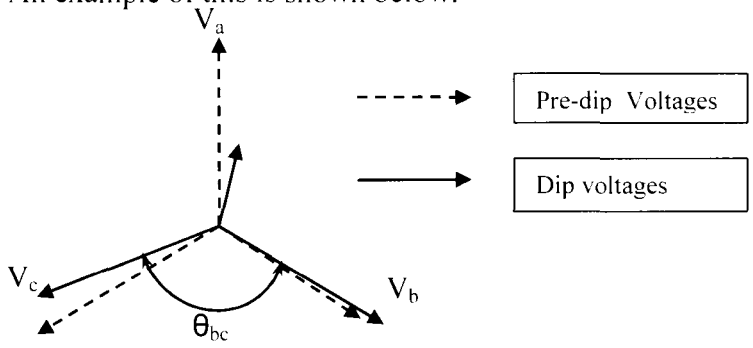

Fig. 4.9 Example of a practically measured dip
which does not match Bollen Dip Types directly

By using the phase angle difference, the new algorithm would be able to classify this dip correctly as a single phase dip (type D_a)

4.9 SHORTCOMINGS OF NEW ALGORITHM

- The new algorithm does not present any information on the magnitude or duration of the voltage dip although it is possible to extract the magnitude information during the progression steps of the algorithms.
- The algorithm requires the sinusoidal waveforms or the corresponding voltage vectors to do the classification. The algorithm is unable to deliver a result based solely on RMS voltage values.
- The characteristic voltage V and the PN factor F used in the sequence algorithms are not derived by the new algorithm, since it does not produce the sequence components. The quantification of voltage dips that is achieved with V and F are thus unavailable in the new algorithm.

4.10 SUMMARY

In this chapter, the development and implementation in Matlab™ and Simulink™ of the new classification algorithm is described in detail. In contrast to the Bollen classification algorithms, it does not transform the input voltages to an analysis domain. The dip types are derived directly, based on the relationships between the measured voltage magnitudes and phase angles. The Ziarani algorithm is used to extract the phase angle of the input voltages.
The new algorithm is able to classify dip types which do not match the Bollen dip types exactly. This is a as a result of using the phase angle difference as a decision-making criterion. By using Matlab™ built-in functions, dip classification algorithms can be adapted easily for application to sinusoidal or RMS measurements.

In the chapters which follow, the new algorithm is evaluated by software simulation, laboratory experimentation as well as by its application to actual measured dips from the Eskom distribution network.

CHAPTER FIVE

EVALUATION OF PHASE-BASED CLASSIFICATION ALGORITHMS BY MATLAB™ SIMULATION

The dip classification results of the Bollen algorithms under phase shift conditions have been published in [18]. The unsatisfactory performance of the Bollen algorithms under these conditions warrants the use of phase shift as a test variable for evaluating the new algorithm. The literature also indicates a limitation in the Bollen algorithms when the value of the reference angle used in the vector description is set to 0° [18]. In this Chapter, the new algorithm will be evaluated and compared with the existing phase-based algorithms.

The Matlab Simulink™ package will be used as the simulation platform for this evaluation.

5.1 OBJECTIVE OF SOFTWARE SIMULATION

The objective of the software simulation is to evaluate the new algorithm with respect to:

- The impact of phase shift
- The impact of different dip magnitudes
- The impact of reference angle

The new algorithm's results are compared to published results for the Symmetrical Component Algorithm and the Six-Phase Algorithm developed by M Bollen. The Matlab™ functions which implement the Bollen algorithms were provided by Dr Melanie Schilder.

5.2 SIMULATION METHODOLOGY

The methodology used in the simulation was developed to realize the objectives defined in 5.1.
The test parameters were chosen as follows:

5.2.1 Phase Shift

The magnitude of the phase shift on the a-phase was varied from 0° to 360° for single-phase dips (type D_a). For phase-phase dips (type C_b), the phase angle between phases a and c was varied between 0° and 120°). The increment for phase shift was set at 10°.

5.2.2 Dip Magnitude

The dip magnitude was varied from 10% to 90% in increments of 10%.

5.2.3 Reference Angle

To test this parameter, a type D_a dip was simulated at a fixed magnitude of 50%, while the reference angle was varied between 0° and 360° in steps of 10°.

The following types of dips were used in this simulation

- Type D_a – Single phase fault. V_a was selected as the symmetrical phase while V_b and V_c were fixed at 100% magnitude at angles of ± 100° respectively.

- Type C_b – Phase-phase fault. V_b was chosen as the symmetrical phase, while V_a and V_c were chosen as the faulted phases. Both the faulted phases were reduced to the same magnitude value, while V_b was fixed at 100% magnitude and 0° phase angle.

In the simulations performed in this chapter, each test point represents a dip of a certain magnitude and phase shift. A vector containing the voltage magnitudes and phase angles for each test point was created in Matlab™. The test points for the full range of phase shift and dip magnitude were then assembled into a matrix. The classification algorithms were then applied to this matrix and the results saved.

For the reference angle test a matrix of test points was constructed, each representing the same type of dip (D_a), at various values of the reference angle.

5.3 SIMULATION RESULTS

In this section, the simulation results for the dip types described in section 5.2 are presented. The classification results of the Bollen algorithms are shown first, whereafter the results of the new algorithm are shown for the same set of test parameters. The results are shown as three-dimensional surface plots. The test parameters, magnitude and phase shift are plotted on the x and y-axis, while the algorithm output are represented as integer values on the z-axis.

5.3.1 Simulation Results for Type D_a dip – single phase fault on phase a

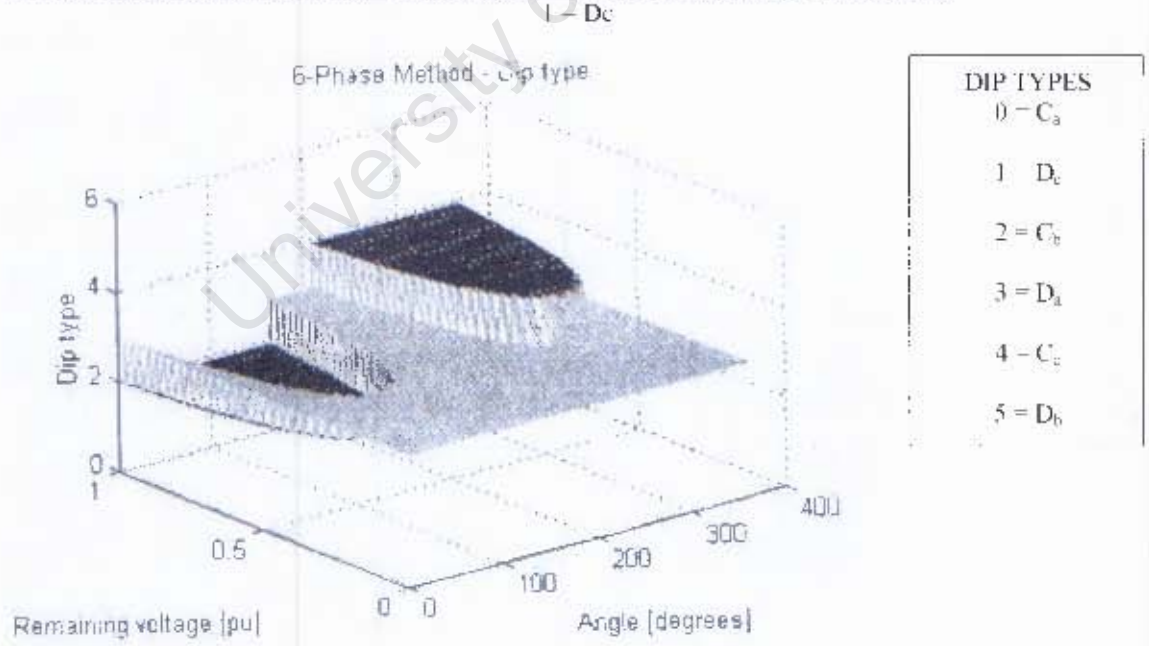

Fig. 5.1 Classification results for dip type D_a Six Phase algorithm *(reprinted from [18])*

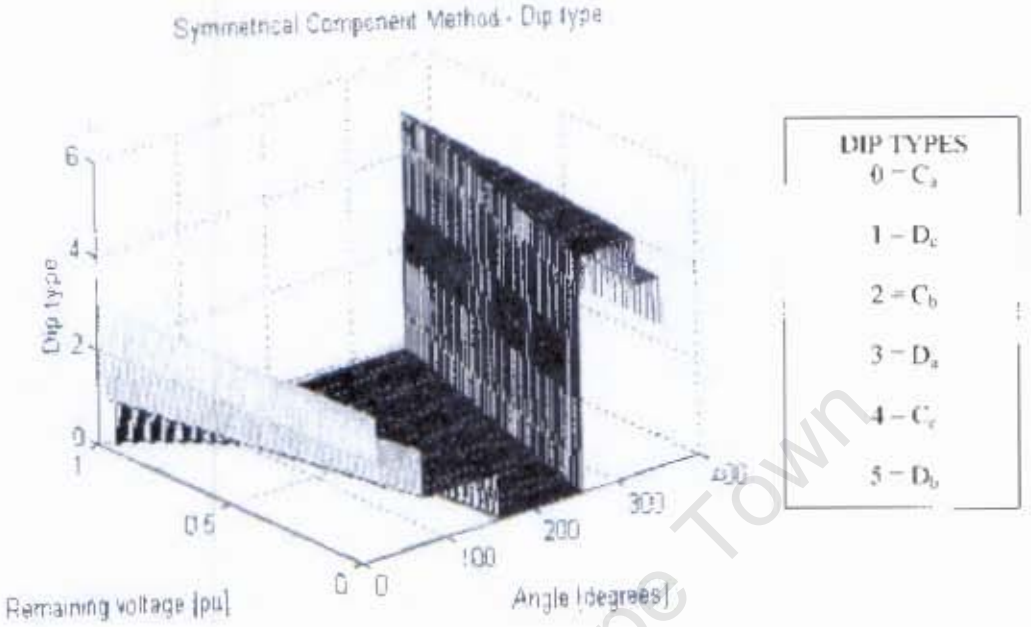

Fig. 5.2 Classification results for dip type D_a – Symmetric Component algorithm *(reprinted from [18])*

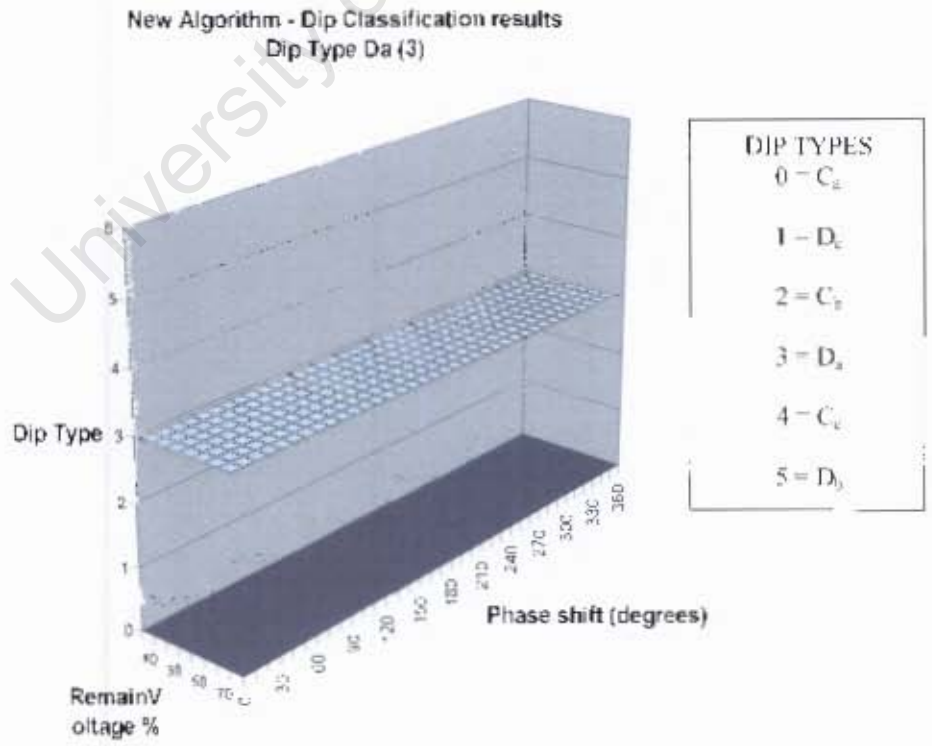

Fig. 5.3 Classification results for dip type D_a – New Algorithm

The classification results for the new algorithm are shown in Fig. 5.3 where the integer value 3 corresponds to Dip Type D_a. It can be seen that the new algorithm gives the correct result (3) for the full range of magnitude and phase shift values.
Comparatively, the symmetrical algorithm and six phase algorithm gives incorrect results over a significant range of phase and magnitude, as shown in Fig. 5.1 and 5.2

This result proves the robustness of the new algorithm to phase shift. This is as expected since the new algorithm uses the difference in phase angles between the healthy phases rather than the absolute phase angle value of any voltage.

5.3.2 Simulation Results for Type C_b dip – phase to phase fault on phases a and c

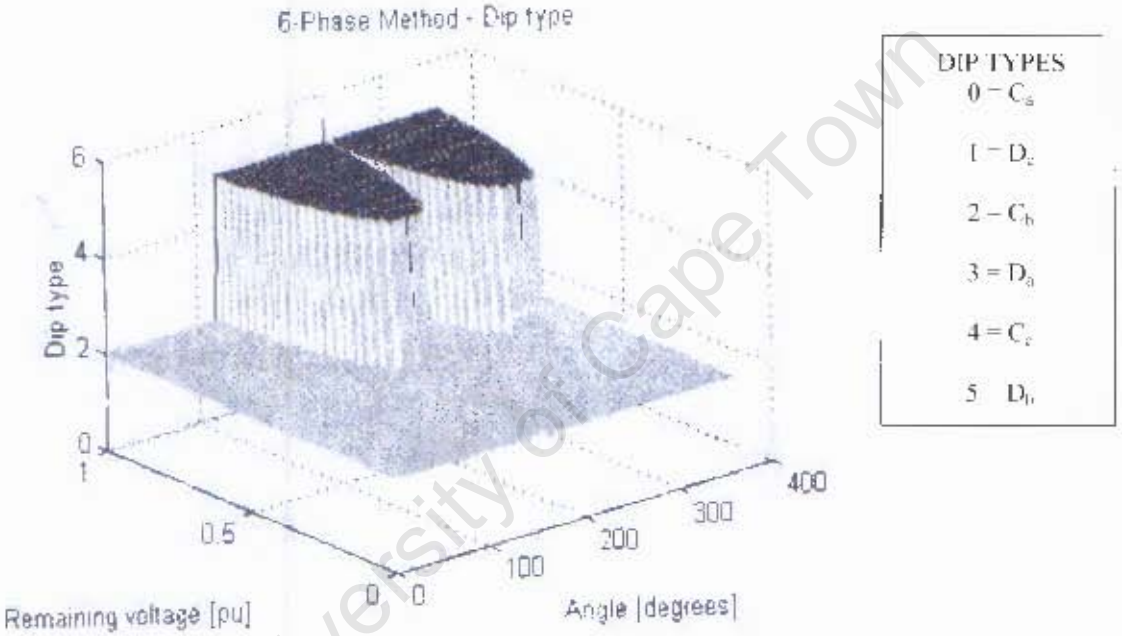

Fig. 5.4 Classification results for type C_b dip– six phase algorithm *(reprinted from [18])*

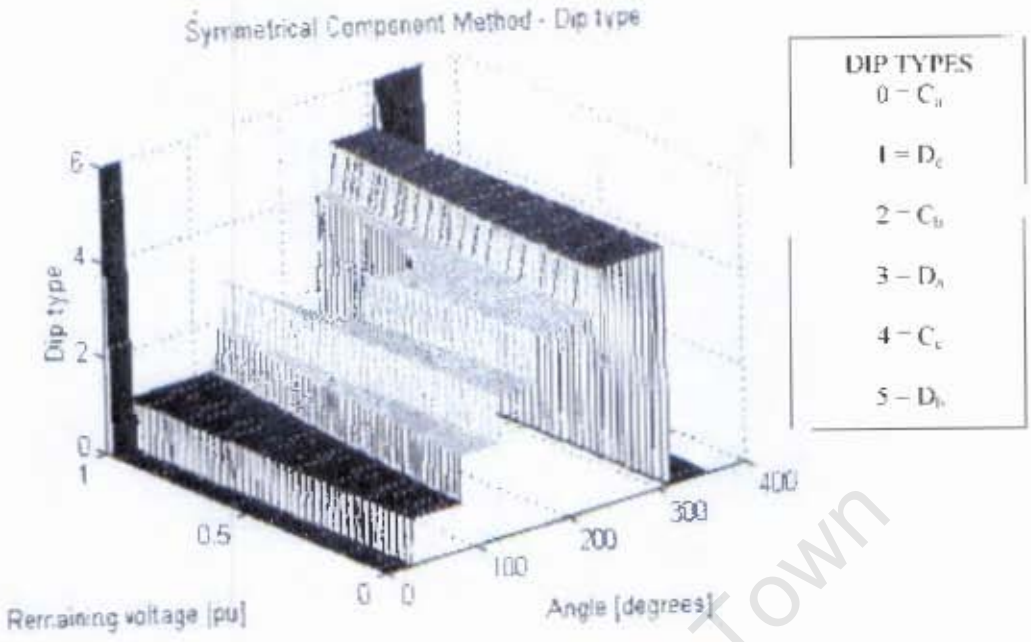

Fig. 5.5 Classification results for type C_b dip– Symmetrical Component algorithm *(reprinted from [18])*

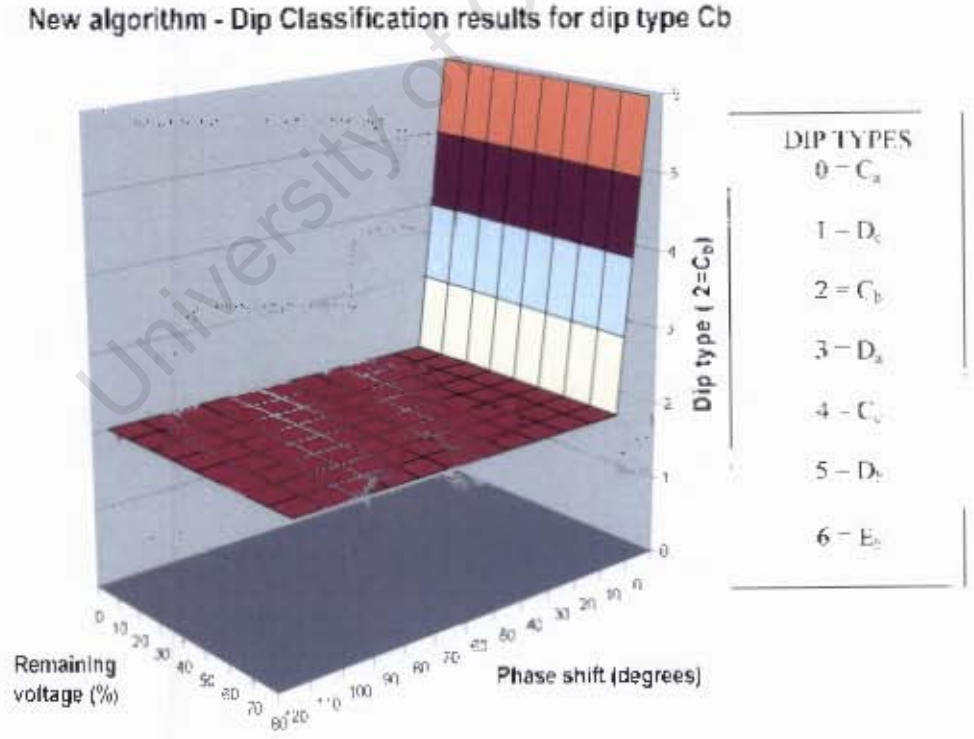

Fig. 5.6 Classification results for type C_b dip – New algorithm

Fig. 5.6 shows the simulated results of the new classification algorithm. The simulated dip type (C_b) corresponds to an integer value of 2 on the z-axis. It can be seen that the new algorithm gives the correct result for most values of phase shift and magnitude. The value of 6 (type E_b) was obtained at a phase shift of 0°. This result appears anomalous, but it is in fact correct since the vector plot of a two-phase fault without phase shift corresponds to that of a type F_a dip as shown in fig. 5.8

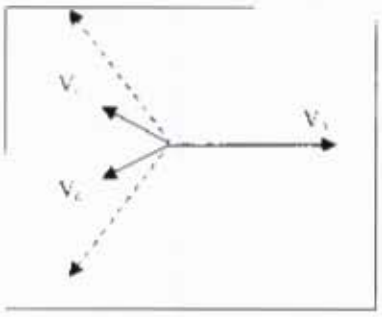

Fig. 5.7 Type C_b dip with phase shift

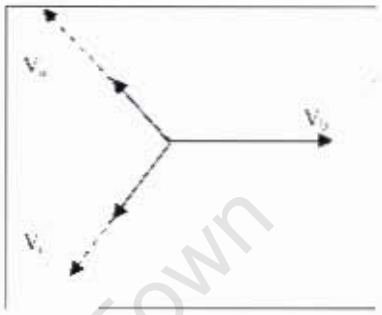

Fig. 5.8 Type C_b dip with zero phase shift = Type F_b

The reprinted results from [18] for the same dip type as classified by the six phase and symmetrical algorithms, show a large range of deviation from the correct result (Fig. 5.4 and Fig.5.5).

5.3.3 Impact of Reference angle

In this simulation, the new algorithm was tested for consistency under conditions of varying reference angle.

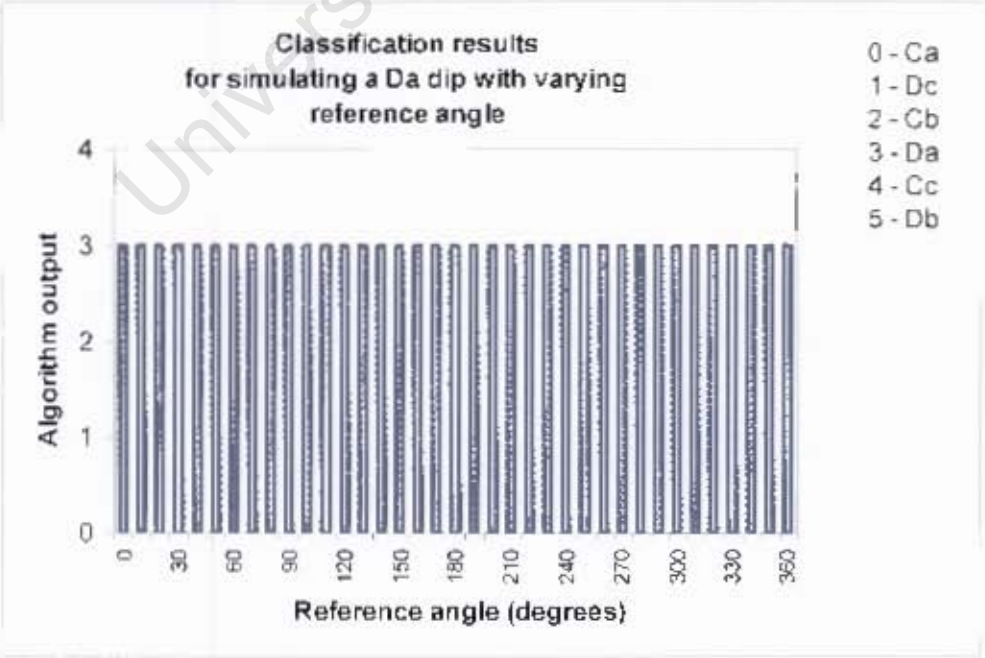

Fig. 5.9 Classification result for varying reference angle – New Algorithm

In the above simulation, a type D_a dip was presented to the new algorithm for classification. The value of the reference angle was varied between 0° and 360°. It can be seen that the new algorithm gives the correct result over the full range of reference angle values. This result is to be expected since the new algorithm does not depend on the absolute rotation of the voltage vectors but the angular difference between the voltage vectors.

5.4 SUMMARY

In this chapter, software simulation has shown that the new algorithm has better classification accuracy than the Bollen algorithms for type C and D dips in the presence of phase shift. Simulations also prove that the new algorithm gives consistent results when classifying a type D dip at various values of reference angle. The new algorithm is also able to make a distinction between all seven Bollen types, unlike the sequence component based algorithms which only distinguish between three of the dip types.

CHAPTER SIX

EXPERIMENTAL VALIDATION OF NEW ALGORITHM

This chapter describes the laboratory component of the research which was conducted in the Machines Laboratory of the UCT Electrical Engineering Department.

The objectives of this experiment are to demonstrate the following:

1. The simulation of voltage dips in a laboratory environment
2. The real-time measurement and storage of dip data.
3. The application of the new algorithm to the classification of laboratory dips

A critical component of the laboratory experiment is the requirement to create voltage dips of known phase shift and magnitude. The measured dip voltages can then be processed by a computer which is loaded with the classification algorithm.

6.1 CREATING VOLTAGE DIPS IN A LABORATORY

Voltage dips are not easily simulated in a laboratory environment. In [3], Keus (et al) describes an IGBT-based programmable power supply which is capable of producing complex voltage dips.
Another popular method for creating voltage dips include switching between various tappings of a multi-tap transformer. In these instances, there is no fault current associated with the voltage dip and the dip in voltage is purely synthesized.

For the purpose of this experiment, a method was devised using the existing equipment in the UCT Machines Laboratory. In practice, voltage dips are caused by a sudden flow of an abnormally high current.
It was thus decided to create a voltage dip in the laboratory, by triggering the flow of a fault current from a three phase generator. This is done by switching one (or more) of the phases to earth via a known impedance. The voltage drop caused by this abnormal current flowing through a predetermined impedance causes a dip in the normal voltage. The magnitude and duration of the dip is controlled by the value of the total fault impedance and the duration of the dip is controlled by a timed switching pulse.

A measurement system simultaneously records the dip voltage waveforms. The recorded waveforms can then be post-processed and applied to the new classification algorithm. Figure 6.1 illustrates the proposed experiment.

6.2 INTERFACING MATLAB™ ALGORITHM WITH DIP MEASUREMENTS

One of the powerful features of MATLAB™ is the compatibility between the Simulink™ simulation tool and the real-time application toolbox.
This functionality allows Simulink™ models and Matlab™ functions to be compiled into code which can be run as real-time applications via an I/O board which consists of a number of Analog to Digital and Digital to Analog converters.

In addition real-time data can be measured and read in to the PC, from where it can be used as input to the software algorithm.
The new algorithm bases its results on the two aspects of the measured waveforms, i.e.

- The relationships between the RMS voltage magnitudes – This is obtained by calculating the RMS values of the measured waveforms on a running window of one cycle of the fundamental 50Hz frequency.
- The phase angle differences between the three voltages – The Ziarani algorithm is used to extract the phase angles of the measured waveforms.

6.3 EXPERIMENTAL SETUP

To implement the experiment, a dc motor was coupled mechanically to a three-phase 10kVA ac generator. The dc motor was driven by a 6-pulse DC converter drive, which enabled the speed of the dc motor to be accurately controlled.
The ac generator was rated at 10kVA, 400V / 230V. To establish a load current, a variable three phase resistive load of 68Ω was connected in delta configuration to the AC supply.

A power electronic switch (triac, type BTA40) was used as a controlled switch to create a fault by shorting one (or more) of the phases to earth. A dSPACE™ RTI (Real Time Interface) system is used to interface the computer with the analog machines.
A control circuit was implemented using opto-triacs (MOC3010) to optically isolate the dSPACE™ output from the generator voltage.
The dSPACE™ real-time interface system is available in Matlab™ as a separate toolbox. Using the ADC and DAC blocks, a measurement and control system was created in Simulink™. This model was then compiled and loaded onto the dSPACE I/O module as a real-time application.
The fault switch pulse was also controlled from the real-time model.

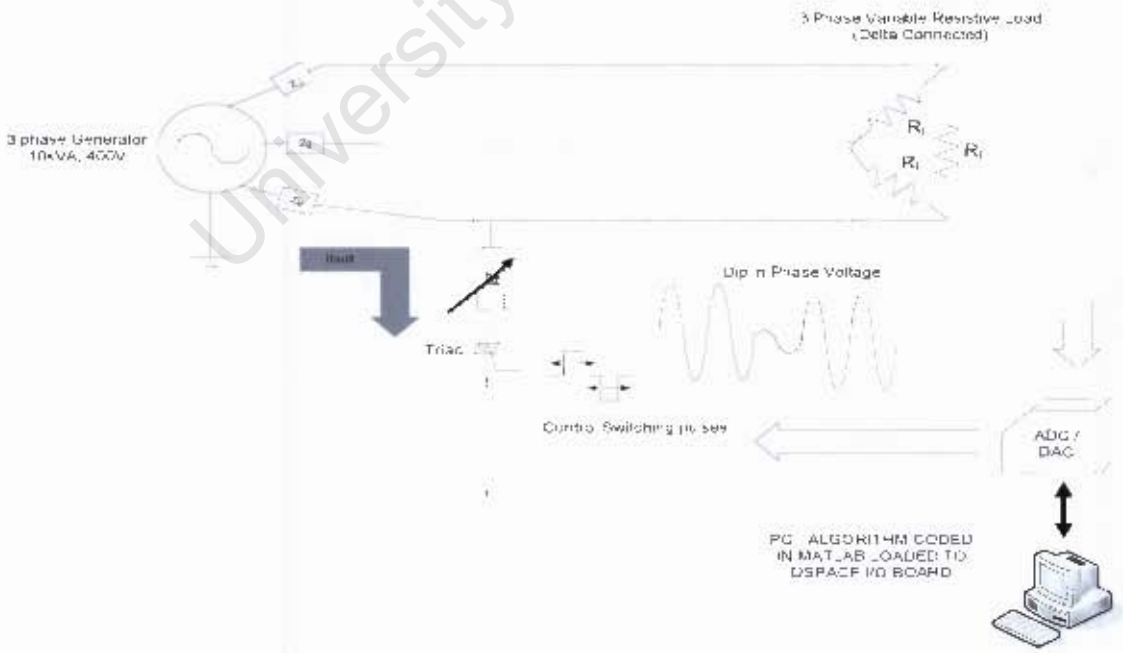

Fig. 6.1 Schematic for creating a Voltage dip in the laboratory

In order to isolate the dSPACE™ analog output from the generator voltage, it was necessary to introduce a control circuit. The optocoupler triac (MOC3010) is ideally suited for this function, since the optical output of the LED is used to trigger the triac into a conductive state.
The dSPACE™ output was programmed to provide a step function which steps between 0V and −10V. The duration of the dip could then be determined from the length of the square wave.

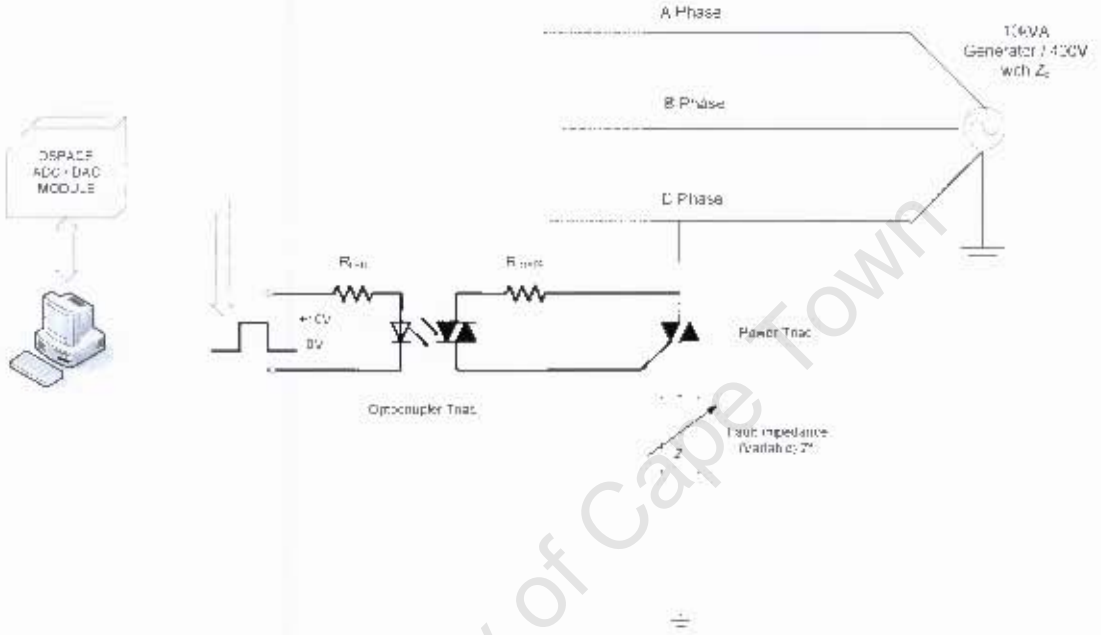

Fig.6.2: Control circuit for switching dips

6.3.1 Voltage Transducer

The voltage was measured using a LEMS transducer module, which scales down voltages in the +-400V range to +-10V. The voltage transducer modules are readily compatible with the I/O board of the dSPACE™ system. Co-axial cables were used from the secondary side of the transducer modules to the interface board.
The three measured voltages were thus scaled down and read into the PC via A/D converters.

6.3.2 Measurement Configuration

Dip voltages can be measured in either wye (phase-phase) or star (phase-neutral) measurement configuration. In [12], the wye method is preferred when it is required to measure the impact on end user equipment. The star method is opted for when it is required to measure the system impact of the dip.
Both methods were used in this experiment to demonstrate the effect of different measurement configurations.

6.4 DATA CONDITIONING OF RMS VOLTAGE VALUES

The measured sinusoid waveforms were read into the computer as described above and passed to a control algorithm running in real time. The purpose of this algorithm was to measure the real-time rms and phase angle values. From the initial measurements, it was seen that the rms voltage signals were polluted with high frequency components as shown in Fig. 6.3

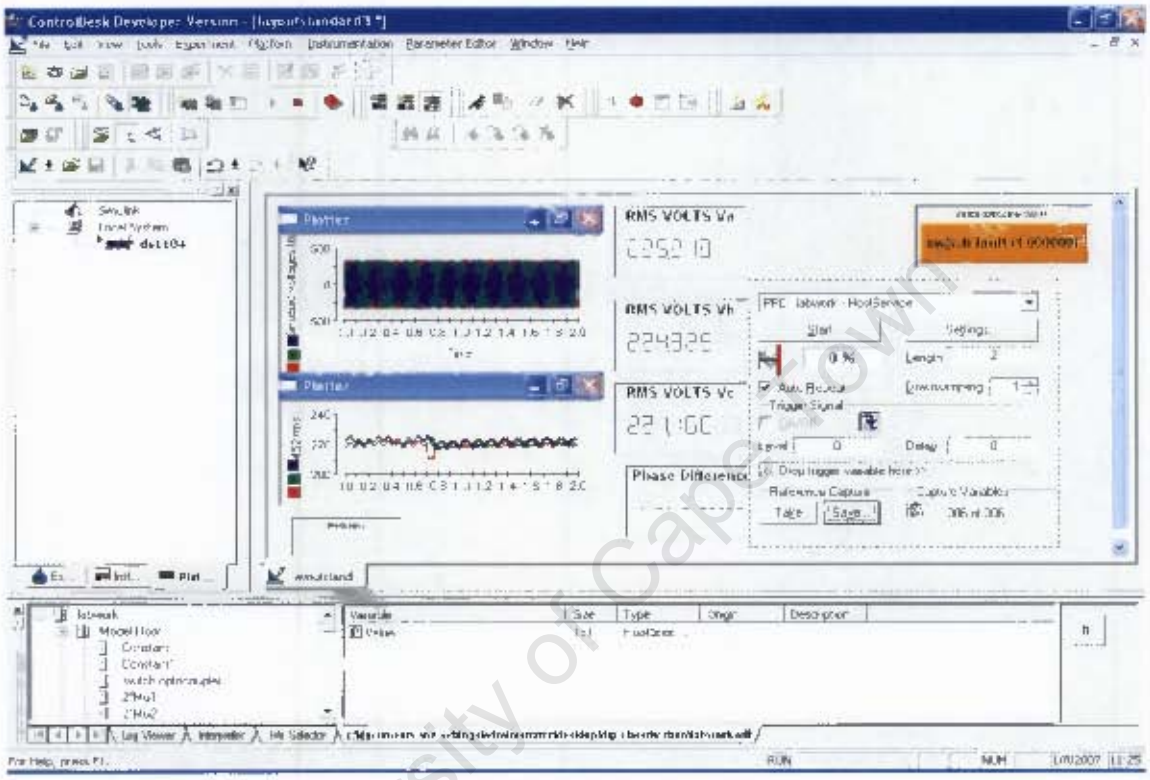

Fig. 6.3 Screendump of initial voltage measurements using DSPACE™ / ControlDesk™

When the input sinusoids were observed on an oscilloscope, the disturbance was not present. It was thus deduced that the unwanted component was introduced by the RMS operation performed by the control algorithm. To eliminate this "noise", a running-average operation was performed on the output of the RMS block. This acted as a low pass filter which cancelled the higher frequency components. A suitable averaging interval of 1/15 seconds was arrived at by trial and error. A smaller averaging window resulted in the higher frequency components not being eliminated while a wider averaging window resulted in the voltage dip itself being smoothed out.
The Simulink™ / dSPACE™ model used for this experiment is shown in Appendix B of this thesis.

6.5 TEST PROTOCOL

The test protocol was aligned with the objectives of the experiment which were to demonstrate;

- The simulation of voltage dips in a laboratory environment
- The real-time measurement and storage of dip data.

- The application of the new algorithm to the classification of laboratory dips

Besides creating dips of significant magnitude, it was also required to simulate significant phase shift. No specific magnitude and phase shift values were stimulated.
Since all the unbalanced dip types defined by Bollen are essentially built on single phase and interphase faults, it was considered sufficient to simulate single phase and phase to phase dips.
The dip voltage waveforms would then be captured and stored for postprocessing. This method allowed greater control since the data could be manipulated (if required) before the classification algorithm was applied.

The measurement system was initially tested by measuring the sinusoidal output of the ac generator under normal conditions. This was done to verify the ability of the Ziarani algorithm to extract the phase angle information. This exercise also enabled the adjustment of data conditioning parameters. The figure below shows the achieved waveform, prior to adjusting the waveform frequency to 50Hz.

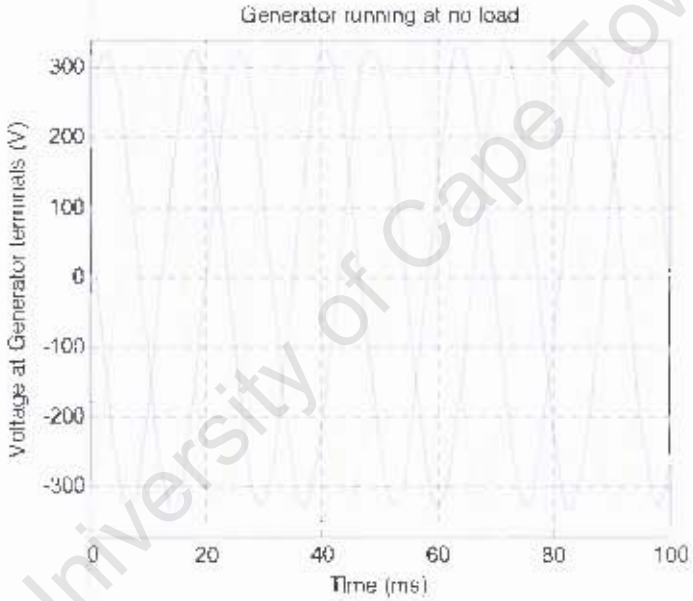

Fig. 6.4 AC Generator output

6.6. LIMITATIONS OF LABORATORY EXPERIMENT

6.6.1 Unexpected Voltage behaviour

The voltage RMS profiles of the laboratory dips do not match the rectangular rms profiles typically experienced on actual networks as shown in Fig. 6.5. This does not affect the accuracy of the new algorithm. Despite switching the fault impedance onto a single phase, all three voltages are reduced in Dip #2. Although this leads to unexpected phasor behaviour, the classification algorithm still gives the correct result for the phasors presented as its input.
In both dips presented in this chapter, the voltage recovery after the dip has a non-rectangular characteristic, in comparison to the dips normally measured on actual networks, as shown in Fig. 6.5.

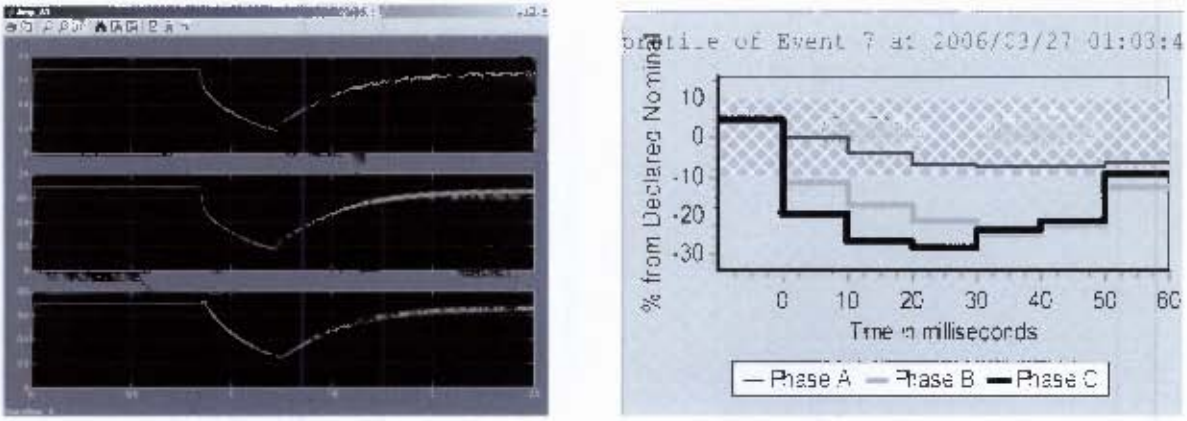

Fig. 6.5 – Comparison between RMS plots of laboratory dips (left) and Transmission network dips (right)

To interpret the dip waveforms above, a dip can be considered as being the result of a fault current flowing through an (fault) impedance.
In the two scenarios depicted in Fig. 6.5, the fault impedances differ. In the case of the Eskom Transmission network, the impedance includes the power station generator as well as the high voltage transmission network. In the laboratory experiment, the fault impedance consists solely of the impedance of the ac generator, which has a higher ratio of inductance. These differences in impedances give rise to the different response waveforms.
The non-rectangular waveform can thus be ascribed to the transient characteristic of the generator impedance.

6.6.2 Ziarani algorithm μ parameter settings

The Ziarani algorithm which is used for phase extraction in this experiment has three adjustable parameters (μ_1, μ_2 and μ_3) which determine the balance between speed and accuracy of the algorithm [2]. In the initial stages of this experiment, it was attempted to adjust the parameters to obtain a satisfactory balance between the two opposing features. It was found that the phase values output by the Ziarani algorithm showed an unsatisfactorily large variance for certain ranges of input voltage magnitudes and parameter values. The problems of spurious outputs and parameter selection were referred by the author to Mr. Ziarani, (via email on 20th January 2007).
Mr. Ziarani responded as follows:

> *"That doesn't surprise me. The mu (μ) parameters need to be very carefully selected to yield correct results..."*

Based on trial and error, it was found that the following values gave satisfactory results when the input signal was normalized to 1.

TABLE 6.1 PARAMETER SETTINGS OF ZIARANI ALGORITHM

Parameter	Value
μ_1	20
μ_2	0.04
μ_3	4000

6.7. EXPERIMENTAL RESULTS

The results are presented as a number of time-based plots showing the various outputs of the laboratory experiment.

6.7.1 Voltage Dip #1 – Phase-phase fault between phases a and c

In this simulation, a phase-phase dip was created by switching a resistive impedance of 5Ω between phases a and c. Table 6.2 summarises the experimental parameters used in this simulation.

TABLE 6.2 EXPERIMENTAL PARAMETERS FOR PHASE-PHASE FAULT

Experimental parameters	
Type of fault	phase-phase
Voltage Measurement method	phase-neutral
Max. Δ Phase Difference	36°
Fault Impedance	5 Ω
Peak Fault Current	51 A
Resistive load prior to dip	0 Ω
Simulation Duration	2500 ms

A peak fault current of 51A was measured between phases a and c using a clip-on ammeter. The maximum phase shift measured was 36°.

Fig. 6.6 shows the scaled RMS voltages which were recorded for this dip. It can be seen that the two faulted phases are reduced while the voltage on the unfaulted phase is also reduced although to a lesser extent. The reduction in voltage on the unfaulted phase is unexpected, but it is due to the inductive behaviour of the generator.

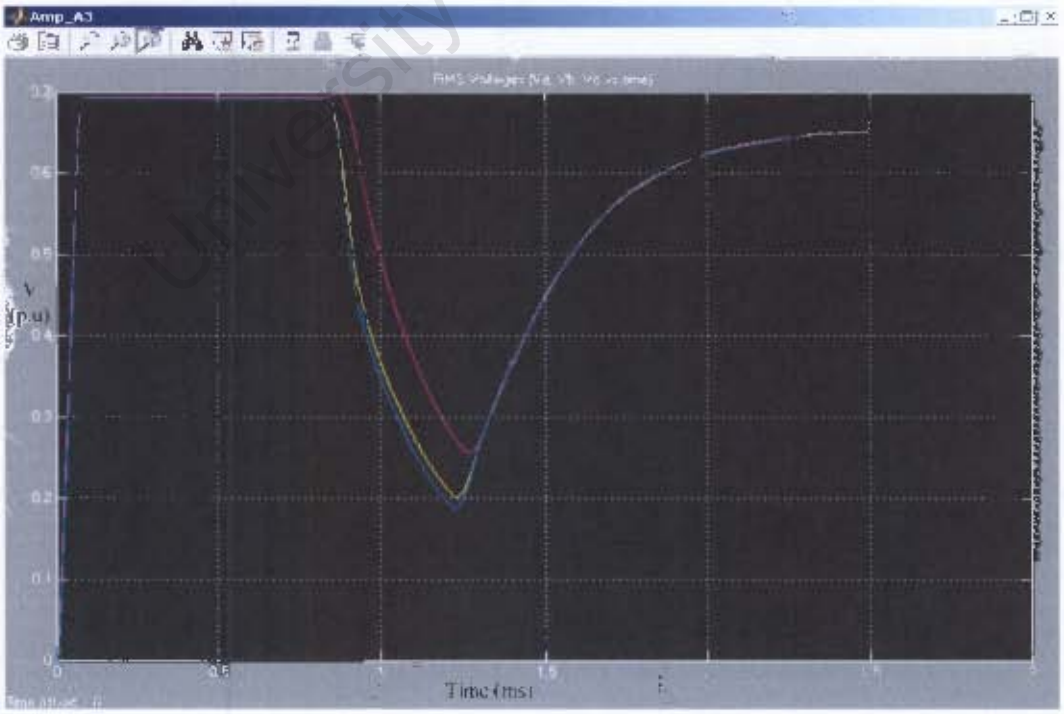

Fig. 6.6: Dip 1 – Scaled RMS Voltage profile of phase-phase dip

Fig.6.7 shows the values for the phase angle difference between phases a and b (θ_{ab}) and phases a and c (θ_{ac}). These values are obtained from the outputs of the Ziarani algorithm which is used to track the phase angle of each voltage. It can be seen that the Ziarani algorithm behaves as expected; taking 100ms to latch onto the signal and tracking it closely thereafter. From the trace of θ_{ac_a} maximum phase shift of 36° is noted.

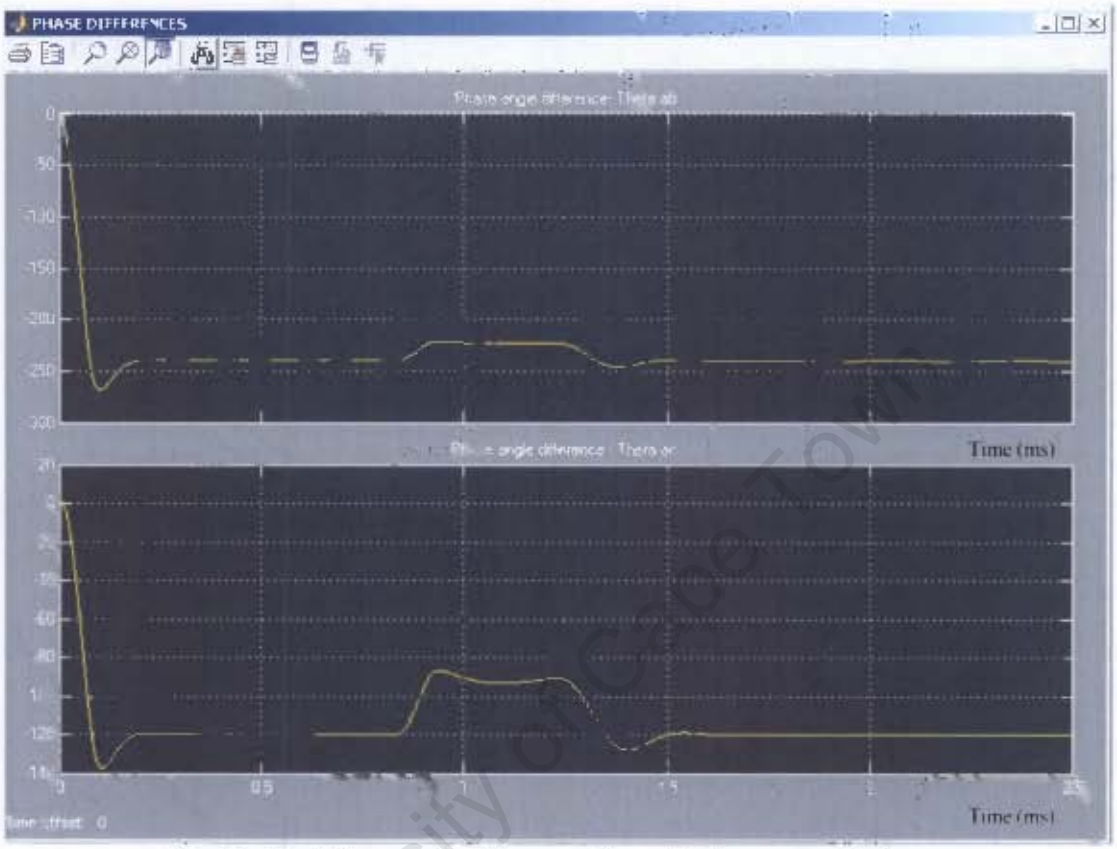

Fig. 6.7: Dip 1- Phase angle differences (θ_{ab} and θ_{ac}) – measured in degrees

Fig.6.8 and 6.9 show the phasor plots of the three voltages before and during the simulated dip. The phasor plot during the dip clearly indicates the reduction on phases a and c.

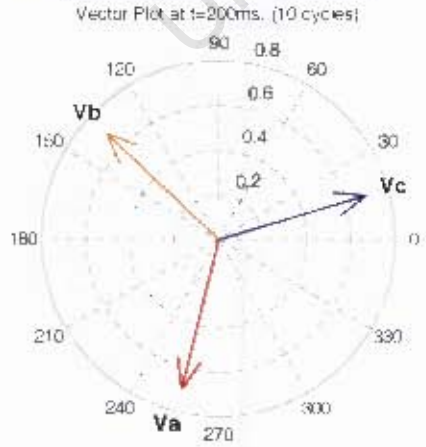

Fig. 6.8: Phasor plot before dip (t=200ms)

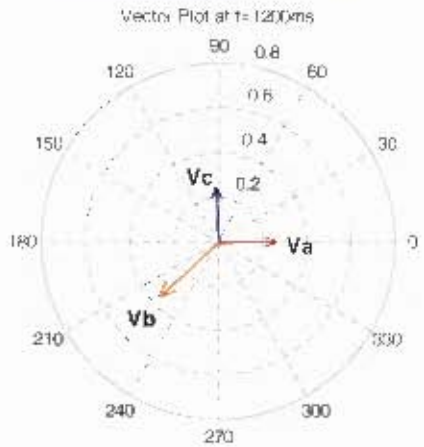

Fig.6.9 Phasor plot during dip (t=1200ms)

The measured voltages in Fig 6.6 and the phase values in Fig.6.7 were captured and presented to the new algorithm for classification. The table below summarises the classification results of the new algorithm for this dip.

TABLE 6.3 CLASSIFICATION RESULTS FOR DIP #1

New Algorithm	
Time (ms)	**Classification result**
t<920	no dip
920<t<980	Cb
1000<t<1360	Gb
1380<t<2220	A

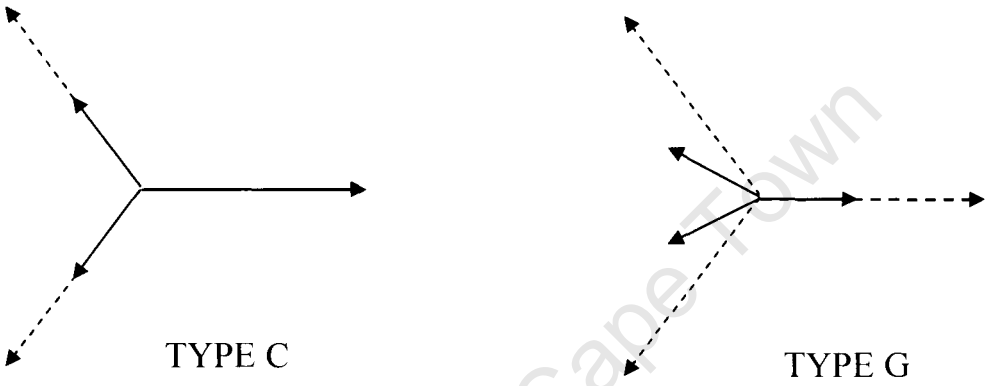

Fig. 6.10 Phasor plots for Dip types C and G

The vector plots of fig. 6.8 and 6.9 confirm the correctness of the classification algorithm for a phase-phase fault. The correct results were obtained despite the significant rotation of all three vectors during the dip. This is as expected, since the algorithm uses the phase difference (fig. 6.7) for classification. Figure 6.10 shows the phasor plots for the algorithm results. After t= 1380ms, the phasors exhibit the behaviour of a Type A dip as seen in Fig.6.6. The new algorithm correctly classifies the voltages during the dip.

6.7.2 Voltage Dip #2 - Phase to Neutral Fault on phase c

In this simulation, a dip was simulated by switching a resistive impedance of 5Ω between the c-phase and the neutral phase. Table 6.4 summarises the experimental parameters used in this simulation.

TABLE 6.4 EXPERIMENTAL PARAMETERS FOR PHASE--NEUTRAL FAULT

Experimental parameters	
Type of fault	phase-neutral
Voltage Measurement method	phase-neutral
Max. Δ Phase shift	35°
Fault Impedance	5 Ω
Peak Fault Current	54 A
Resistive load prior to dip	0 Ω
Simulation Duration	1000ms

In this simulation, a peak fault current of 54A was measured using a clip-on ammeter. The maximum phase shift measured was 35°.

Fig. 6.11 shows the scaled RMS voltages which were recorded for this dip. It can be seen that the voltage on the faulted phase is reduced while the voltages on the unfaulted phases are also reduced although to a lesser extent. The reduction in voltage on the unfaulted phases is due to the inductive behaviour of the generator. In Fig.6.11, the fault impedance was removed at t=650ms. The profile thereafter represents the voltage recovery of the AC generator.

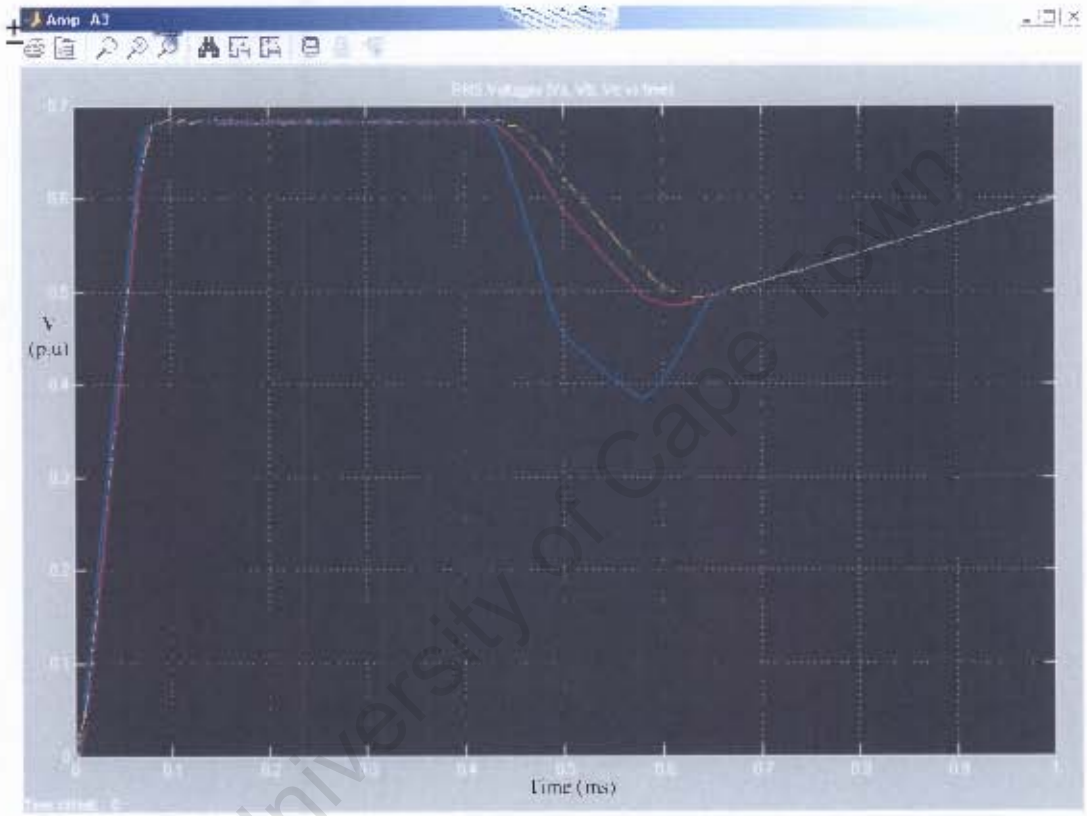

Fig. 6.11: Dip #2 – Scaled RMS Voltage profile of phase-neutral dip

Fig.6.12 shows the values for the phase angle difference between phases a and b (θ_{ab}) and phases a and c (θ_{ac}). These values are obtained from the outputs of the Ziarani algorithm which is used to track the phase angle of phase voltage. It can be seen that the Ziarani algorithm behaves as expected; taking 100ms to latch onto the signal and tracking it closely thereafter.

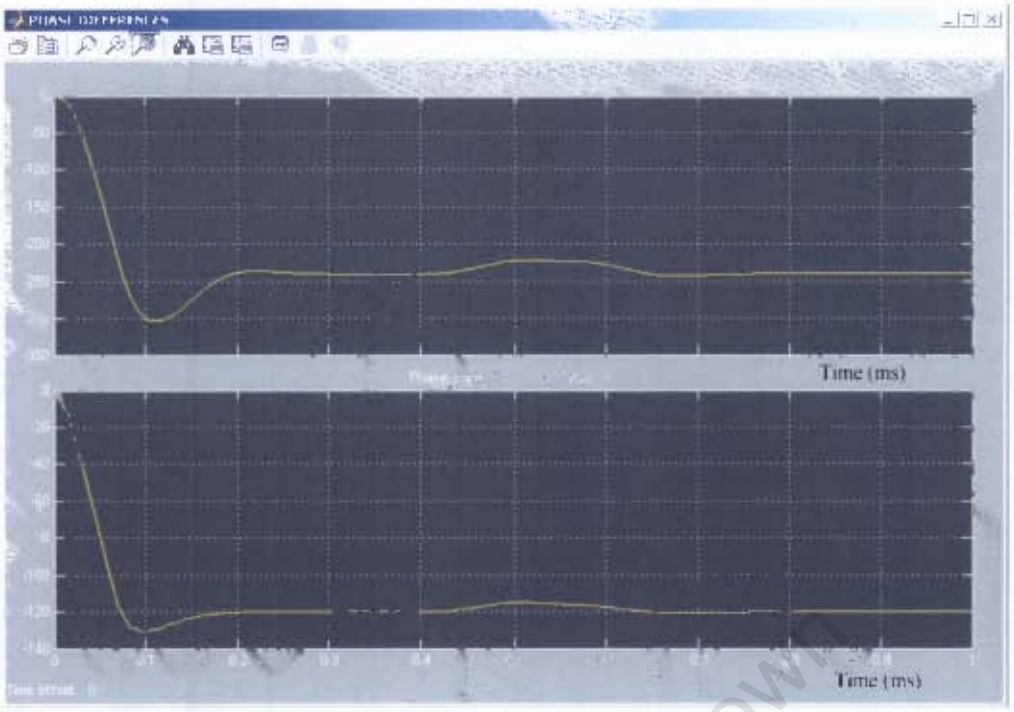

Fig. 6.12 Dip #2- Phase angle differences (θab and θac) – measured in degrees

Fig.6.13 and 6.14 show the phasor plots of the three voltages before and during the simulated dip. The phasor plot during the dip clearly indicates the reduction on phase c.

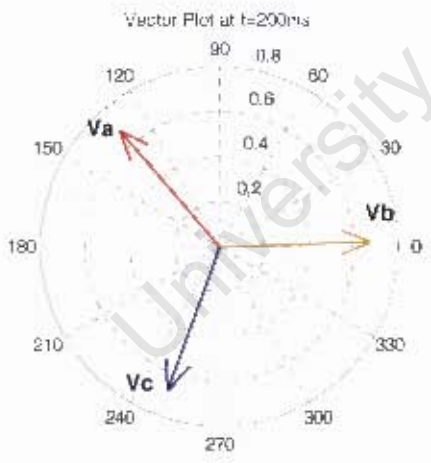

Fig. 6.13: Phasor plot before dip (t=200ms)

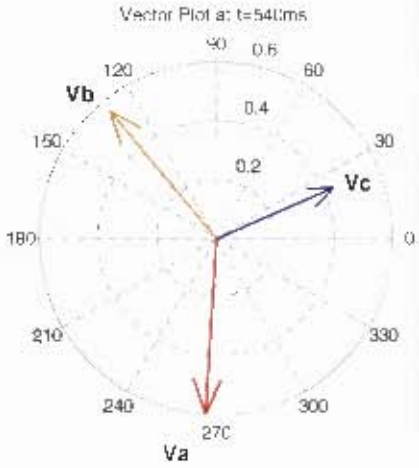

Fig. 6.14 Phasor Plot during dip (t=540ms)

The values recorded in Fig. 6.11 and 6.12 were captured and post-processed before sending it to the classification algorithm. The results of the classification algorithm are summarized in Table 6.5. It is seen that the new algorithm returned a classification result of type F_c over the duration of the fault. This result corresponds to the voltage phasor relationships as shown in Fig. 6.14.

TABLE 6.5: CLASSIFICATION RESULTS FOR DIP #2

Classification Algorithm result	
Time (ms)	**Classification result**
t<480	no dip
500<t<640	Fc
660<t<1000	A

The classification algorithm correctly identifies the dip type during the dynamic behaviour of the fault. It is also seen that the voltage recovery after the dip is correctly classified as a three phase dip.

6.8 SUMMARY

Within a limited range of parameters, dips of various types can be simulated in a laboratory by switching known fault impedances onto the output of a generator source. A limitation of this form of dip creation is that the rectangular dip profiles commonly found in actual networks are not obtained, due to the effects of simulating the faults close to the generating source. For the purpose of verifying the new classification algorithm, the experimental procedure described in this chapter provided an easy method of generating dips.

With the proper set of parameters, the Ziarani algorithm can be used to track the phase angles during dip waveforms satisfactorily.
The application of the new classification algorithm to laboratory dips has been verified. The algorithm classified the measured dips correctly, in terms of dip type as well as the symmetrical phase as per the Bollen phase-based definitions.

CHAPTER SEVEN

APPLICATION OF THE NEW ALGORITHM TO THE CLASSIFICATION OF ESKOM DIPS

This chapter describes the application of the new algorithm to the classification of actual voltage dips as measured at two sites on the Eskom Distribution Network.

7.1 DIP MEASUREMENTS IN ESKOM

In line with the requirements of the NER, Eskom operates a power quality measurement system which covers all voltage levels. The measured data includes voltage profiles, harmonics, unbalance and voltage dips. Most of the recording instruments are automatically downloaded via different communication media (such as GPRS modems and X.25 networks) and the data is automatically exported to a central database.
As a means of converting the data to usable information, measured voltage dips are matched to known network events in order to identify the origin and cause of the dip. This exercise is commonly called "dip-to –trip matching". The database enables Eskom to perform a host of tasks related to power quality, such as mandatory power quality reporting, power quality contract management, statistical studies and customer trends etc.

7.2 DIP RECORDING INSTRUMENT

One of the popular instruments used for dip recordings is the Vectograph™. Aside from recording the voltage rms values over time, a profile of the voltage phase behaviour during the dip is also recorded. For the purpose of this experiment, it is necessary to extract this phase information and present it to the classification algorithm.

7.3 TRIAL SITE DATA

The data set used in this exercise was measured at the following site:

- Airport substation 11kV Busbar – this substation supplies mainly industrial consumers via underground cable and overhead line feeders.

The site measured dips originating from Transmission faults at higher voltage levels (132kV and 400kV) as well as faults on the 11kV reticulation networks. The Vectograph™ recorder is connected to the secondary side of the voltage transformers in four-wire (star) configuration.
The data set consisted of the dips recorded from 01 February 2006 to 30 April 2006
In order to test the application of the algorithm, four dips were selected from the dataset for classification.

7.4 DATA MANIPULATION TO ENABLE ALGORITHM COMPATIBILITY

The classification algorithm requires the RMS magnitude and phase angle values of the three phases over a time interval. This information is contained in a file created by the VectoGraph Export™ Utility; a software routine which stores the magnitude and phase angle for vector events over a one-cycle (20ms) averaged interval. In order to extract the required data, the raw data file (.rev) is "exported" using the export program. The resultant file is then manually manipulated using Microsoft Excel™ to create a matrix of magnitude and phase values which represents the dip behaviour.

This matrix is then read into Matlab™ and fed to the classification algorithm.

7.5 TEST PROTOCOL

It was decided to consider the measured dips in relation to the cause of the dip. Using this approach, the following fault origins were extracted:

1. Transmission Line Faults
2. MV (11kV) Equipment Failure
3. Faults on Customer cables

7.6 LIMITATIONS OF ALGORITHM APPLICATION TO ESKOM DIPS

7.6.1 Dip type Classification of Multistage Faults

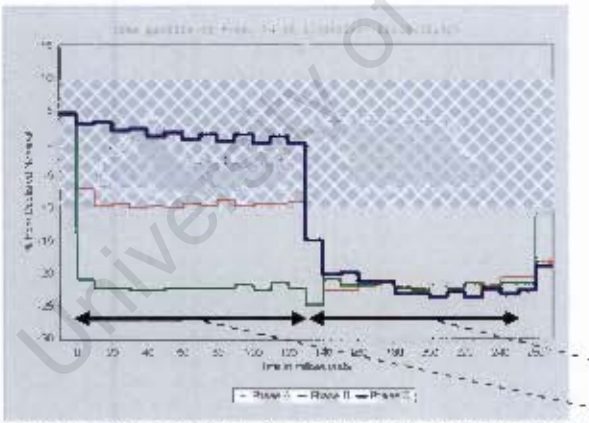

Fig 7.1 Example of an actual dip displaying more than one dip type

The above dip originated due to a fault on an 11kV overhead line which is renowned for tree and bird incidents. When considering this dip, it is evident that the characteristics of more than one dip type manifests as the fault develops. This behaviour is particularly common on overhead line faults where a dip may start as a single phase fault which progresses to a dual-phase or three phase fault. Faults caused by tree contacts commonly display this type of behaviour. The phenomenon of multistage dips has been recorded in literature, but no attempts have been made to classify such dips. The new algorithm proposed in this thesis does not attempt to provide a single classification for this type of dip.

7.6.2 Shortcomings of new algorithm

It was found that the new algorithm is unable to classify a dip correctly when the voltage magnitudes are not clearly matched to the relationships shown below.

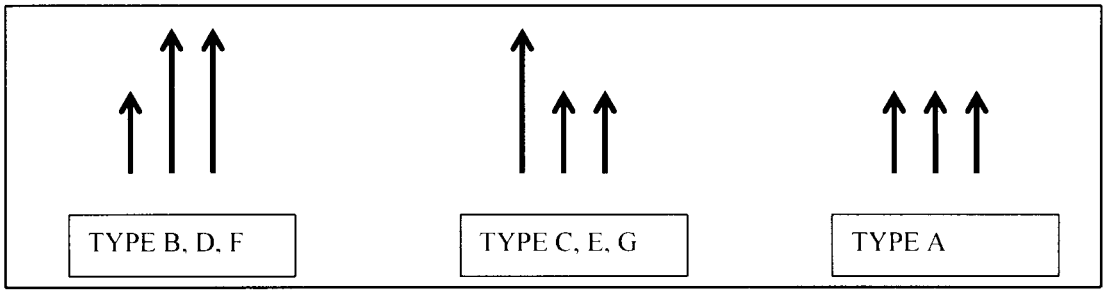

Fig. 7.2 Relationships between voltage magnitudes for various dip types

If the differences between the three voltage magnitudes are roughly equal, the new algorithm is unable to match the magnitude. This anomaly arises as follows:
The algorithm sorts the three voltages in ascending order to give $[V_x, V_y, V_z]$ with V_z having the highest magnitude. The following relational test is then used to match the magnitude relationship to a dip type, as shown in the figure above.

$$If\ V_z - V_y > V_y - V_x\ then.....$$

If the differences between the voltages are equal, the algorithm is unable to match the dip type and returns a "no match" result. This was found to be the case for the dip presented in 7.7.4

7.7 CLASSIFICATION RESULTS

The results are presented by first showing the RMS voltages during the dip and a plot of the voltage phasors at a specific time interval. Both of these plots are taken directly from the Vectograph™ recorder. The output of the classification algorithm is then shown in tabular format, with a classification result for each 20ms time interval.

7.7.1 Transmission (400kV) Line Fault

The details of this dip are shown in Table 7.1

TABLE 7.1 DIP DETAILS FOR TRANSMISSION LINE FAULT

Measurement Location	Airport substation - 11kV busbar
Date/Time:	27/3/2006 at 01:03:46AM
Fault Origin	Droerivier Hydra No2 400kV Line Fault

Fig. 7.1 shows the dip due to a line fault on a Transmission line. The fast protection settings limits the dip duration to 60ms. The recording instrument outputs the dip vector

information in 20ms averaged intervals, which are then processed by the classification algorithm as explained earlier in this chapter.

It can be seen that phases b and c are reduced in magnitude below the 90% threshold level. This indicates a phase-phase fault between the two phases. The correct classification for this dip would be Type C_a

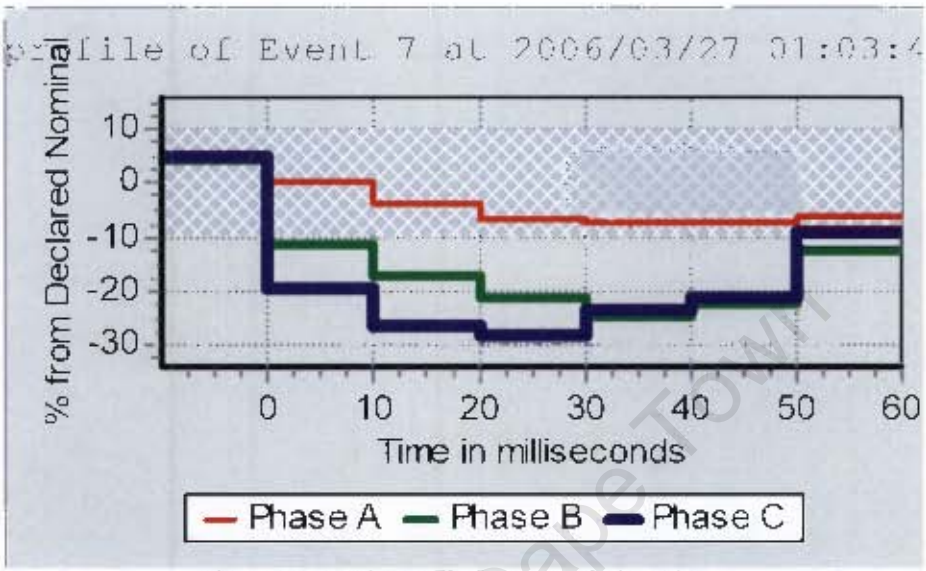

Fig. 7.3 RMS Dip Profile for Transmission Dip

In Fig.7.2. the phasor plot of the voltages is shown for the time interval (0-20ms). By comparing this phasor plot to the Bollen dip types, it is clear that this is a Type C_a dip.

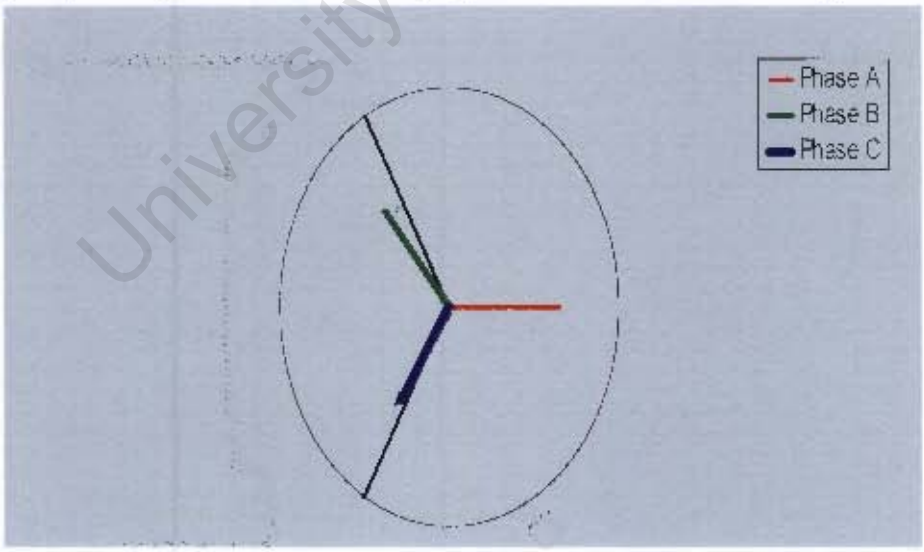

Fig.7.4 Typical Vector Plot (0ms – 20ms)

In Table 7.2. the values presented to the new algorithm and the classification results are presented. It is seen that the new algorithm gives the expected result over the duration of the dip. The moderate values of phase shift during the dip are to be expected for transmission networks, as mentioned in Chapter 2.

Fig. 7.6 and 7.7 show the voltage phasor plots during the two stages of the dip. By matching these phasors with the Bollen dip types, it can be seen that the first stage of the dip is Type C_a dip and the latter portion of the dip is type A.

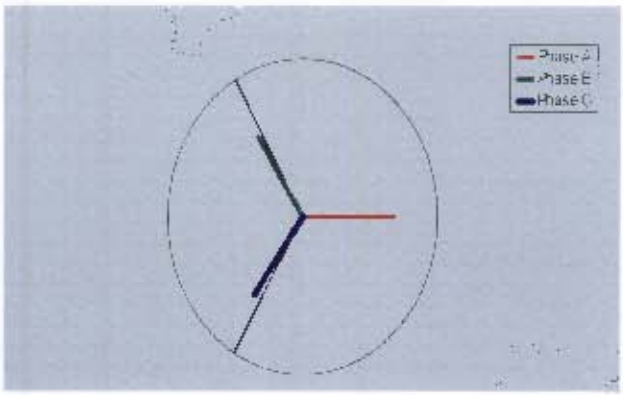

Fig. 7.6 Typical Vector Plot (0-100ms)

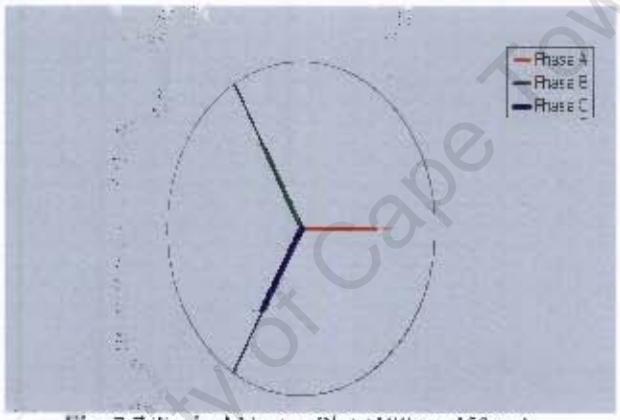

Fig. 7.7 Typical Vector Plot (100ms-450ms)

Table 7.4 shows the magnitude and phase values obtained from this dip and the results of the classification algorithm

TABLE 7.4: AVERAGED VALUES OF VOLTAGE MAGNITUDE (% OF NOMINAL) AND ANGLE DURING DIP

Time interval (ms)	Va	Angle a	Vb	Angle b	Vc	Angle C	New Algorithm output	Phase Shift (max degrees)
0	100.7	180	89.4	302.9	91.4	54.5	TYPE Ca	5.5
20	100	180	88.7	302.8	90.4	54.2	TYPE Ca	5.8
40	99.3	180	88.4	303	91.1	54.3	TYPE Ca	5.7
60	97.7	180	90.1	303.5	89.4	56.4	TYPE Ca	3.6
80	84.7	180	85.4	299.9	85.4	60	TYPE A	0.1
100	83.4	180	84.1	299.4	84.8	59.6	TYPE A	0.6
120	83.4	180	84.4	299.4	84.1	59.9	TYPE A	0.6
140	83.4	180	84.1	299.8	84.4	60	TYPE A	0.2
160	83.1	180	83.8	299.6	84.1	59.7	TYPE A	0.4
180	82.7	180	83.4	299.4	84.1	59.6	TYPE A	0.6
200	82.4	180	83.8	299.5	84.4	59.7	TYPE A	0.5
220	83.1	180	83.8	299.8	84.1	60	TYPE A	0.2
240	82.7	180	83.8	299.3	83.8	59.7	TYPE A	0.7

260	82.7	180	83.8	299.3	84.1	59.5	TYPE A	0.7
280	83.1	180	83.4	299.2	84.1	59.6	TYPE A	0.8
300	82.4	180	83.4	298.9	84.4	59.2	TYPE A	1.1
320	83.1	180	83.8	299.3	85.1	59.4	TYPE A	0.7
340	83.7	180	83.8	299.2	84.8	59	TYPE A	1
360	83.4	180	83.4	300.3	83.1	59.3	TYPE A	0.7
380	84.7	180	86.4	300.8	84.8	60.6	TYPE A	0.8
400	85	180	86.4	300.9	84.8	60.4	TYPE A	0.9
420	84.7	180	86.4	301	84.4	60.8	TYPE A	1
440	85.4	180	86.8	301.3	84.4	60.6	TYPE A	1.3

Table 7.4 Cont.

It is evident that this dip is not homogenous with regards to its classification. Initially the fault has the characteristics of a phase to phase (type Ca) fault which then progress to a three phase fault (type A). This is likely due to the transitive behaviour of the flashover fault.

The algorithm is able to distinguish between the two types and gives a correct output. The maximum phase shift that was measured is 5.8 degrees.

7.7.3 Dip due to Pollution-induced Flashover on 400kV Transmission line

The details of this dip are shown in Table 7.5

TABLE 7.5 DIP DETAILS FOR TRANSMISSION FAULT

Measurement Location	Airport substation - 11kV busbar
Date/Time:	18 Feb. 2006 at 21:36
Fault Origin	Pollution-induced flashover on 400kV Muldersvlei / Droerivier 2 line

Fig. 7.8 shows the RMS profile of this dip. The dip magnitude is 60% and the duration is 100ms From the RMS profile, it is seen that the fault caused a single phase dip on the b-phase.

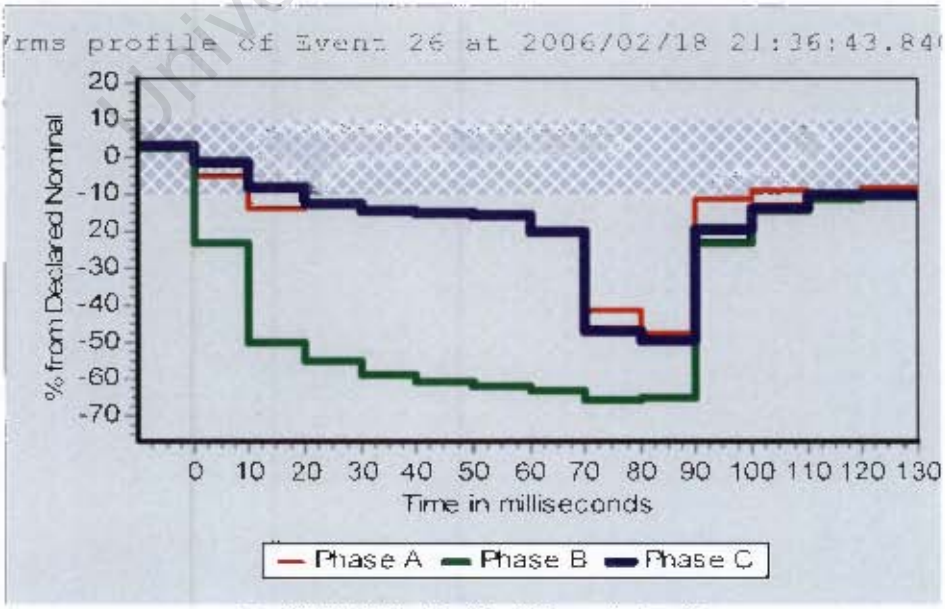

Fig. 7.8 RMS Dip Profile of Transmission dip

Fig. 7.9 shows the voltage phasor plot at t=80ms. This clearly shows the single phase nature of the fault with the b-phase as the symmetrical phase. From this figure, the correct classification should be a type F_b dip.

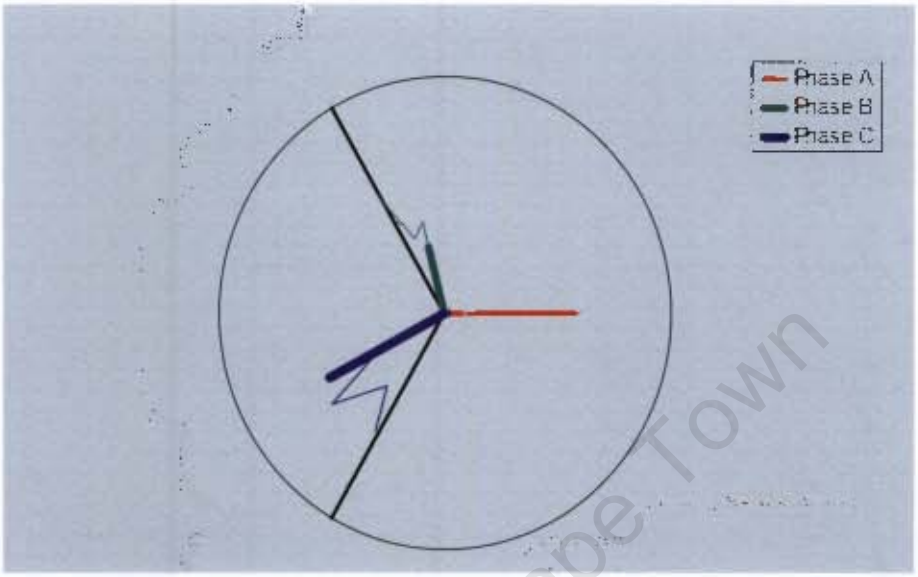

Fig. 7.9 Typical Vector plot (t=80ms)

Table 7.6 presents the classification results for this dip. The new algorithm correctly classifies the dip. It is noted that a significant phase shift (33.6°) occurs during this dip. This amount of phase shift is uncommon for Transmission line faults and is probably due to the nature of the flashover which occurred.

From Fig.7.6 it is deduced that at t=90ms the protection system operated a circuit breaker which interrupted the fault current. The algorithm returns a type Ca result at t=100ms. This result may be correct in terms of the phasor relationships at that time, but it is not indicative of the fault since it occurs after the fault current has been interrupted.

TABLE 7.6 AVERAGED VALUES OF VOLTAGE MAGNITUDE AND ANGLE DURING DIP

Time interval (ms)	Va	Angle a	Vb	Angle b	Vc	Angle C	Algorithm output	Phase Shift (max degrees)
0	89.7	180	59.6	284.6	94.7	37.3	NO MATCH FOUND	22.7
20	86	180	43	284.4	86.4	28.6	TYPE Fb	31.4
40	84.4	180	39.1	283.6	84.4	26.4	TYPE Fb	33.6
60	63.1	180	33.8	283	54.3	30.3	TYPE Fb	29.7
80	61.5	180	51.3	292.8	59.3	50.3	TYPE Fb	9.7
100	90.7	180	87.1	300.9	88.1	58	TYPE Ca	2

7.7.4 Dip due to cable fault

The details of this dip are shown in Table 7.7

TABLE 7.7 DIP DETAILS FOR CABLE FAULT

Measurement Location	Airport substation - 11kV busbar
Date/Time:	13 March 2006 at 14:44:18
Fault Origin	11kV Cable Fault on customer network

Fig. 7.9 shows the RMS profile of this dip. The dip magnitude is 50% and the duration is 550ms From the RMS profile, it is seen that the fault initially appears as a single phase fault which develops into a two phase fault.

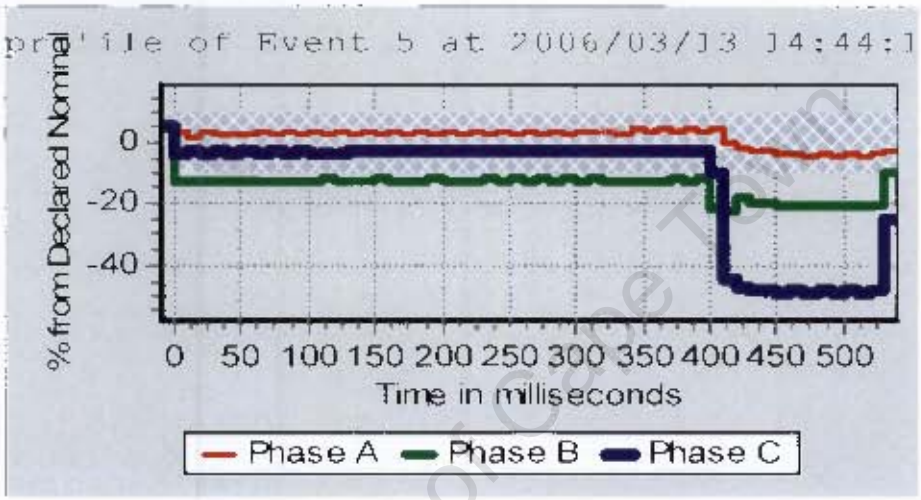

Fig. 7.9 Dip RMS plot of cable fault dip

Fig. 7.10 below displays the voltage phasors at t 420ms. The phasors indicate a phase-phase fault which would lead to a classification of either Type C, E or G.

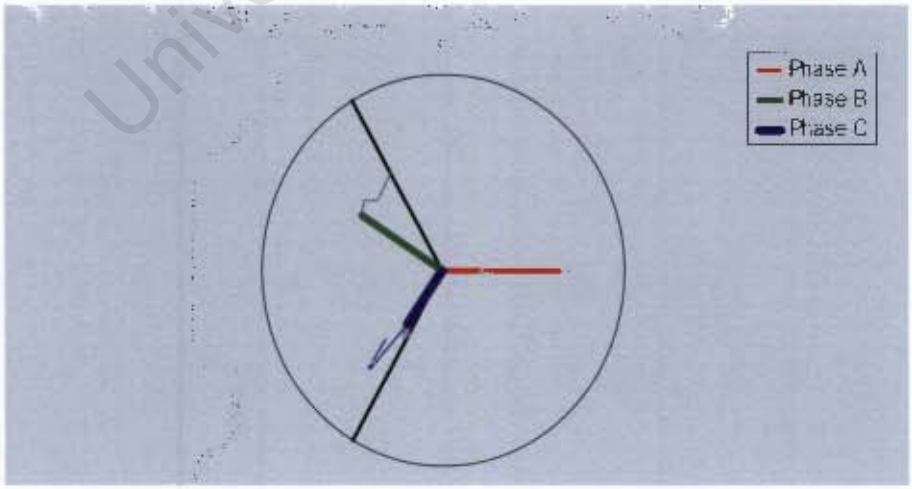

Fig. 7.10 Typical Vector Plot (400ms – 520ms)

The classification results for this fault are shown in Table 7.8. As expected, the algorithm returns a type D_6 dip for the first portion of the dip (up to 400ms).

TABLE 7.8 AVERAGED VALUES OF VOLTAGE MAGNITUDE AND ANGLE DURING DIP

Time (ms)	va	theta a	vb	theta b	vc	theta c	Algorithm output	Phase shift
0	102.7	180	87.7	298.8	97	51.2	**TYPE Db**	8.8
20	102.7	180	88.1	299.1	97	51.3	**TYPE Db**	8.7
40	102.3	180	87.7	298.5	96.7	51.1	**TYPE Db**	8.9
60	102.7	180	87.7	298.9	96.7	51.3	**TYPE Db**	8.7
80	102.7	180	87.7	298.8	96.7	51	**TYPE Db**	9
100	102.7	180	88.1	299.1	96.7	51.4	**TYPE Db**	8.6
120	103	180	88.1	299	97	51.1	**TYPE Db**	8.9
140	102.7	180	87.7	299.2	97	51.1	**TYPE Db**	8.9
160	103	180	88.1	299	97	51	**TYPE Db**	9
180	102.7	180	88.1	299	97.4	50.9	**TYPE Db**	9.1
200	103	180	88.1	299	97	51	**TYPE Db**	9
220	103.3	180	87.7	299.2	97	51.1	**TYPE Db**	8.9
240	103.3	180	87.7	298.9	96.7	50.9	**TYPE Db**	9.1
260	103	180	87.7	298.9	97	50.8	**TYPE Db**	9.2
280	103.3	180	88.1	298.9	97	51.1	**TYPE Db**	8.9
300	103.3	180	88.1	299.1	97	50.9	**TYPE Db**	9.1
320	103.7	180	88.1	299	97	50.9	**TYPE Db**	9.1
340	103.3	180	88.1	299.1	97	50.9	**TYPE Db**	9.1
360	103.3	180	87.7	299.1	97.4	50.9	**TYPE Db**	9.1
380	103.7	180	88.1	299.1	97.4	50.9	**TYPE Db**	9.1
400	101.7	180	76.5	315.1	71.5	47.8	**TYPE Ca**	15.1
420	97.7	180	81.5	327.4	52	54.5	**NO MATCH**	27.4
440	96.7	180	80.5	327.7	51.3	54.1	**NO MATCH**	27.7
460	96	180	80.1	327.6	51.3	54.1	**NO MATCH**	27.6
480	96	180	80.1	327.6	51	54.3	**NO MATCH**	27.6

From 420ms – 520ms, the algorithm fails to categorise the dip into any of the dip type categories and produces a "No Match" result. It is noted that during this portion, the phase shift is in excess of 20°. However, it is not the phase shift that results in the erroneous result; rather it is the difference between the minimum and maximum voltages. This is explained in 7.6.2

7.8 SUMMARY

In this chapter it has been shown that the data format used by Eskom's Power Quality recorders can relatively easily be integrated with Matlab™ algorithms for the purpose of dip classification.
The occurrence of 'multistage' dips, i.e. faults which display more than one dip type, is also presented in this chapter.
It can be investigated whether it is feasible to have more than one dip type classification per dip event. Alternately, it may also be considered to find (statistically) which dip type occurs for the longest time and allocate that as the classification to the entire dip.

The former proposal is more suitable when considering equipment sensitivity. A certain piece of equipment may be susceptible to a dip type which occurs for a small fraction of the

total dip duration. If a single classification is made to the entire dip, this information may be lost if the specific dip type did not occur for the majority of the dip duration.

Although it is not in the scope of this research, the application of the algorithm to a larger data set from the Eskom database would also give valuable insight to the natural occurrence of multistage dips at different voltage levels. It is possible to implement classification algorithms to automatically do the dip-to-trip matching; a task which is currently being manually performed.

The new algorithm's inability to classify dips where the voltage difference between the highest, middle and lowest dip voltages are the same, is made apparent in this chapter. This is a significant finding, since the occurrence of such faults in practice is also verified in this chapter.

CHAPTER EIGHT

CONCLUSION

The research work described in this thesis was aimed at developing a new phase-based dip classification algorithm that would correctly classify voltage dips into the type categories defined by Dr M Bollen. The development and evaluation of the new algorithm highlighted a number of findings which are summarised below. Through this research, directions for further research into this field have also been identified.

8.1 MAIN FINDINGS

- ***Shortcomings of Bollen algorithms***

  The Symmetrical Component method gives incorrect results in the event of phase shift while the Six-Phase method fails if the angle of the reference voltage is set to 0°. The phase shift limitation is critical, since phase shift does occur in practice, more commonly on distribution cable networks. The requirement of the reference angle can be overcome by mathematical manipulation (rotation) of the measured vectors, although it carries a computational overhead.

- ***Suitability of Ziarani algorithm to dip classification***

  The Ziarani algorithm was applied successfully to extract and track the phase angles of dip voltages. However, the sensitivity of the tuning parameters (μ_i) required a process of trial and error to determine suitable values. The algorithm required 100ms of pre-dip voltage to "lock on" to the input signal, whereafter it could track changes in the signal parameters, subject to the speed and accuracy determined by the parameter (μ_i) settings.

- ***New Algorithm***

  The new algorithm proposed in this thesis overcomes the phase shift shortcoming of the Symmetrical Component Algorithm by computing the dip type based on the difference in phase angle between the measured voltages. This also allows the new algorithm to be unaffected by the angle of the reference voltage. From a computational perspective, the new algorithm is more efficient since it does not transform the measured voltages to an analysis domain.

  In phase-based dip classification, seven dip types (A-G) exist. For six of the types (B-G), there are three subtypes; which give rise to eighteen distinct categories (B_a, B_b, B_c,....G_a, G_b,G_c).
  The subtypes are known by the symmetric phase, i.e. the "dipped" phase for single phase dips, and the unaffected phase for phase-phase dips.

- ***Software simulation of new classification algorithm***

  The new algorithm was implemented as series of Matlab™ functions. To simulate sinusoidal dip voltages of varying magnitude and phase, a new Simulink™ model was created (Dip Generator). The software simulation included the Ziarani algorithm which was used to extract the phase angles of the dip voltages. The simulation results showed that the new algorithm is able of classifying type C and D dips across the full range of phase shift and magnitude values.

- ***Laboratory verification of classification algorithm***

  For the experimental simulation, dips were simulated in the laboratory. This was achieved by throwing faults on a three-phase generator supply. The generator and fault circuitry were interfaced with the Classification algorithm via the dSPACE™ real-time simulation package. This method of creating dips in a laboratory was found to be adequate for the purpose of verification. A limitation of this form of dip creation is that the rectangular dip profiles commonly found in actual networks are not obtained, due to the effects of simulating the faults close to the generating source
  It was found that a phase shift of up to 36° could be created from a resistive fault impedance.

- ***Application to Eskom dips***

  The dip data recorded by Eskom's Power Quality recorders (Vectograph™) can relatively easily be integrated with Matlab™ algorithms for the purpose of dip classification. The new algorithm gave correct results when it was applied to a sample of actual network dips. Phase-based dip classification can potentially be used in automated dip-to-trip matching.

8.2 FURTHER RESEARCH

- ***Multistage dips***

  Multistage dips were encountered in the laboratory experiment as well as the Eskom Data. The occurrence of more than one dip type in a single fault incident has been mentioned in the researched literature. It remains to be finalized as to how such dips should be classified. The notion of allocating a single type-classification to a dip is more appropriate when considering equipment immunity. In contrast, a statistical study of dips may require that all dip types which occur during a fault be taken into account.

- ***Shortcomings of new algorithm***

  A critical aspect of the new algorithm is that it uses the relationships between the RMS magnitudes of the three voltages to determine a result. When the differences between the highest, middle and lowest RMS magnitudes are roughly equal, the algorithm gives incorrect results. This shortcoming was made apparent when the algorithm was applied to actual dips measured on the Eskom Distribution network.

In [15], Bollen derives the mathematical relationships between the RMS voltage magnitudes for the various dip types. A solution to the new algorithms shortcoming may be found by changing the decision making criteria to co-incide with the mathematical relationships, as specified by Bollen in [15].

Voltage dips present a multifaceted challenge in terms of equipment performance and the statistical behaviour of power networks. From this perspective, it becomes easy to accept that there cannot be a single definition that applies equally well in all fields.

REFERENCES

[1] A. McEachern, "Designing equipment for world wide power", internet download from www.powerstandards.com, Jan 2005

[2] A.K Ziarani and A. Konrad, "A Method of Extraction of Sinusoids of Time-Varying Characteristics" *IEEE Transactions on Signal Processing, VOL. 84, NO. 8, August 2004*

[3] A.K. Keus, R. Abrahams and J. van Coller, "Analysis of voltage dip (sag) testing of a 15kW PWM variable speed drive", *Proceedings of the IEEE International machines and drives conference*, Seattle, USA, May 1999.

[4] A.K. Keus, R. Abrahams, J. van Coller and R.G. Koch, "*Comprehensive Testing of a Current Source Inverter Drive",* Saupec Conference, January 2004

[5] A.M. Gaouda, M.M.A. Salama, M.R. Sultan, and A.Y.Chikhani,"Power Quality Detection and Classification using Wavelet-Multiresolution Signal Decomposition*" , IEEE Transactions on Power Delivery, Vol 14, No. 4 October 1999*

[6] D.Borras, M. Castilla, N. Moreno, and J.C. Montana, "Wavelet and Neural Structure: A New Tool for Diagnostic of Power System Disturbances", *IEEE Transactions on Industry Applications, Vol 37, No. 1 , January/February 2001*

[7] D.G. Ece and O.N. Gerek, "Power Quality Analysis using an Adaptive Decomposition Structure", International Conference on Power System Transients, IPST 2003, New Orleans, USA

[8] F. Jurado and J.R. Saenz, "Comparison between discrete STFT and wavelets for the analysis of power quality events", *Electric Power Systems Research 62 (2002) 183-190*

[9] I. Boake, I. Smit, R. Koch and T. Hennessy, "Eskom Power Quality Reference Guide", Rev. 2 , April 1996

[10] J. Kyei, "Analysis and design of power acceptability curves for industrial loads", Masters Thesis and Final Project Report,PSERC Publication 01-28, February 2001.

[11] J.M. van Coller and R.G. Koch, "Dip problems and solutions in practical variable speed drives installations", *Proceedings of the First independent LV switchgear and Drives&Control Conference and Exposition*, Johannesburg, 27 – 29 September 2004.

[12] K. Akpinar, P. Pillay and G.G. Richards, "Induction Motor drive behaviour during unbalanced faults" *Electric Power systems Research 36(1996) 131-138*

[13] L.W. Cheock, T.K. Saha, and Z.Y. Dong, "Power Quality Investigation with Wavelet Techniques", School of Information Technology and Electrical Engineering, The University of Queensland, Australia

[14] M. Bollen, "The theory of voltage dip measurement and characterisation", presentation notes CIRED 2005

[15] M. H. Bollen, P. Goossens, and A Robert "Assessment of Voltage Dips in HV-Networks: Deduction of Complex Voltages from the RMS Voltages", *IEEE Transactions on Power Delivery, Vol.19, No. 2, April 2004*

[16] M. Karimi, H. Mokhtari, and M.R. Iravani, "Wavelet Based On-line detection of Power Quality Disturbances", *IEEE Transactions on Power Delivery, Vol. 15, No. 4, October 2000*

[17] M. Kezunovic and Y. Liao, " A new method for classification and characterisation of voltage sags", *Electric Power Systems Research 58 (2001) 27-35*

[18] M. Schilder and R.G. Koch, "Evaluation of a new three-phase dip definition", Saupec 2004

[19] M.H.J. Bollen, "Algorithms for Characterizing Measured Three-Phase Unbalanced Voltage Dips", *IEEE Transactions on Power Delivery*, Vol 18, No.3,July 2003

[20] M.H.J. Bollen, "Characterisation of voltage sags experienced by three-phase adjustable-speed drives", *IEEE Transactions on Power Delivery*, Vol 12, No. 4, October 1997

[21] NER, Power Quality Directive, April 2002

[22] NRS048-2 , Second Edition, 2004

[23] P. Byrne, D. Pillay and R.G. Koch, " The value of power quality customer forums in a regulated environment", *Proceedings of the 17th International Conference on Electricity Distribution,* Barcelona , Spain, 12-15 May 2003

[24] R. Langley, A. Mansoor, B. Fortenberry and T. Cooke, "Evaluation of ride-through systems for variable speed drives", TR-111952, EPRI, Palo Alto, CA, November 1998

[25] R.A. Flores, "State of the Art in the Classification of Power Quality Events, an Overview, unpublished

[26] R.G. Koch, "Power quality management initiatives: standards, regulatory frameworks and incentives, monitoring, contracting and compatibility guidelines", *15th Conference on Electric Power Supply Industry (CEPSI)*, Shanghai, China, October 2004

[27] R.G. Koch, P. Balgobind and E.Tshwele, "New developments in the management of power quality and performance in a regulatory environment", *Proceeding of the IEEE Africon Conference*, George, South Africa, August 2002

[28] R.G. Koch, P. Balgobind, P.A. Johnson, I. Sigwebela, R. McCurrach, D. Bhana, and J.Wilson, "Power Quality Management in a regulated environment : The South African Experience", *Proceedings of the 40th Cigre Paris Session,* Paris, France , September 2004

[29] R.G. Koch, U. Minnaar, South African National Standards Technical Support, Research Report, RES/RR/04/23995, Eskom Holdings - Resources and Strategy Research, 2005

[30] R.M. de Castro Fernandez, and H..D. Rojas, "An overview of Wavelet Transform Applications in Power Systems", *14th PSCC,* Sevilla, 24-28 June 2002

[31] S Q Davies, U J Minnaar, J M Van Coller, R G Koch, "Investigating the Performance of AC Contactors during Voltage Dips", Saupec 2003

[32] S. Santoso and P. Hoffman, "Power Quality Assessment via Wavelet Transform Analysis", *IEEE Transactions on Power Delivery*, Vol 11, No. 2 , April 1996

[33] S. Santoso, W.M. Grady, E.J. Powers, J. Lamoree, and S.C. Bhatt, "Characterisation of Distribution Power Quality Events with Fourier and Wavelet Transforms", *IEEE Transactions on Power Delivery,* Vol. 15, No. 1, January 2000

[34] S. Santoso, E.J. Powers, and W.M. Grady, "Power Quality Disturbance Data Compression using Wavelet Transform Methods", *IEEE Transactions on Power Delivery,* Vol. 12, No. 3, July 1997

[35] T. Anderson and D. Nilsson, "Test and Evaluation of voltage dip immunity", *MSc Thesis - STRI Project no. 3261*, Nov 2002

[36] T. B. Littler, and D.J. Morrow, "Wavelets for the analysis and Compression of Power System Disturbances", *IEEE Transactions on Power Delivery, Vol. 14, No. 2, April 1999*

[37] T.K. Abdel-Galil, M. Kamel, A.M. Youssef, E.F. El-Saadany, and M.M.A. Salama, "Power Quality Disturbance Classification Using the Inductive Inference Approach", *IEEE Transactions on Power Delivery*, Vol 19, No. 4 , October 2004

[38] T.X. Zhu, S.K. Tso, and K.L. Lo, "Wavelet-Based Fuzzy Reasoning Approach to Power Quality Disturbance Recognition", *IEEE Transactions on Power Delivery*, Vol 19, No. 4, October 2004

[39] TLM Format Manual (Draft 0) , Eskom Distribution Power Quality Course, Cape Town, 22 Nov - 26 Nov. 2004

[40] www.powerstandards.com

[41] www.semi.org

[42] Y. Gu and M.H.J. Bollen, "Time-Frequency and Time-Scale Domain analysis of Voltage Disturbances", *IEEE Transactions on Power Delivery,* Vol 15, No. 4, October 2000

[43] A. Sannino, M. H. J. Bollen and J. Svensson, "Voltage Tolerance Testing of Three-Phase Voltage Source Converters", *IEEE Transactions on Power Delivery, Vol. 20, No. 2, April 2005*

[44] J. D. Glover, M.Sarma, *Power System Analysis and Design,* second edition, Boston: PWS Publishing Company, 1994, pp 49-52

APPENDICES

APPENDIX A-1 MATLAB™ FUNCTION CODE FOR NEW CLASSIFICATION ALGORITHM

```
function dip_vector = create_dip_vector(Voltage_vector)
% this function accepts a 5-element vector with 3 RMS phase voltages and 2 phase differences
%and creates a unique 5-element column vector for each dip type.
Vnom =0.707 ;
V_sorted = sort(Voltage_vector(1:3));
theta_ab = abs(Voltage_vector(4));
theta_ac = abs(Voltage_vector(5));
theta_bc = abs(360-(theta_ab+theta_ac));
Vz = V_sorted(3);
Vy = V_sorted(2);
Vx = V_sorted(1);

 %TYPE A DIPS        -closeness of magnitude              angle test
 if (Vz < 0.9*Vnom) && ( abs(Vz-(2*Vy)+Vx)<0.02*Vnom)%&& ( abs(120-((theta_ab+theta_bc)/2)) <3)
   dip_vector=[1,0,0,0,0]; % type A

 %TYPE B DIPS
elseif (Vy>0.9*Vnom) &&(Vz-Vy < Vy-Vx) && (Vx<0.9*Vnom) && (Voltage_vector(1)==Vx)
&&(theta_bc<=120)
dip_vector=[0,1,0,0,0]; %type Ba
elseif (Vy>0.9*Vnom) &&(Vz-Vy < Vy-Vx) && (Vx<0.9*Vnom) && (Voltage_vector(2)==Vx)
&&(theta_ac<=120)
dip_vector=[1,1,0,0,0]; %type Bb
elseif (Vy>0.9*Vnom) &&(Vz-Vy < Vy-Vx) && (Vx<0.9*Vnom) && (Voltage_vector(3)==Vx)
&&(theta_ab<=120)
dip_vector=[0,0,1,0,0]; %type Bc

   % Type C DIPS
elseif (Vz>0.9*Vnom)&& (Vz-Vy>Vy-Vx)&&(Vy<0.9*Vnom) && (Voltage_vector(1)==Vz)&&
(theta_bc<120)
dip_vector=[1,0,1,0,0]; %type Ca
elseif (Vz>0.9*Vnom)&& (Vz-Vy>Vy-Vx)&&(Vy<0.9*Vnom) &&(Voltage_vector(2)==Vz)&&
(theta_ac<120)
dip_vector=[0,1,1,0,0]; %type Cb
elseif (Vz>0.9*Vnom)&& (Vz-Vy>Vy-Vx)&&(Vy<0.9*Vnom) &&(Voltage_vector(3)==Vz)&&
(theta_ab<120)
dip_vector=[1,1,1,0,0]; %type Cc

  %Type D Dips
elseif (Vy>0.9*Vnom) &&(Vz-Vy < Vy-Vx) && (Vx<0.9*Vnom)
&&(Voltage_vector(1)==Vx)&&(theta_bc>120)
dip_vector=[0,0,0,1,0]; %type Da
elseif (Vy>0.9*Vnom) &&(Vz-Vy < Vy-Vx) && (Vx<0.9*Vnom)
&&(Voltage_vector(2)==Vx)&&(theta_ac>120)
dip_vector=[1,0,0,1,0]; %type Db
elseif (Vy>0.9*Vnom) &&(Vz-Vy < Vy-Vx) && (Vx<0.9*Vnom)
&&(Voltage_vector(3)==Vx)&&(theta_ab>120)
dip_vector=[0,1,0,1,0]; %type Dc

  %TYPE E DIPS
elseif (Vz>0.9*Vnom)&&(Vz-Vy > Vy-Vx) && (Vx<0.9*Vnom)&&(Voltage_vector(1)==Vz)
&&(theta_bc==120)
```

```
dip_vector=[1,1,0,1,0]; % type Ea
elseif (Vz>0.9*Vnom)&&(Vz-Vy > Vy-Vx) && (Vx<0.9*Vnom)&&(Voltage_vector(2)==Vz)
&&(theta_ac==120)
dip_vector=[0,0,1,1,0]; % type Eb
elseif (Vz>0.9*Vnom)&&(Vz-Vy > Vy-Vx) && (Vx<0.9*Vnom)&&(Voltage_vector(3)==Vz)
&&(theta_ab==120)
dip_vector=[1,0,1,1,0]; % type Ec

  %TYPE F DIPS
elseif (Vz<0.9*Vnom)&&(Vz-Vy < Vy-Vx) && (Voltage_vector(1)==Vx) &&(theta_bc>120)
dip_vector=[0,1,1,1,0]; %type Fa
elseif (Vz<0.9*Vnom)&&(Vz-Vy < Vy-Vx) && (Voltage_vector(2)==Vx) &&(theta_ac>120)
dip_vector=[1,1,1,1,0]; %type Fb
elseif (Vz<0.9*Vnom)&&(Vz-Vy < Vy-Vx) &&(Voltage_vector(3)==Vx) &&(theta_ab>120)
dip_vector=[0,0,0,0,1]; %type Fc

  % TYPE G DIPS
elseif (Vz<0.9*Vnom)&&(Vz-Vy > Vy-Vx)&&(Voltage_vector(1)==Vz) &&(theta_bc<120)
dip_vector=[1,0,0,0,1]; %type Ga
elseif (Vz<0.9*Vnom)&&(Vz-Vy > Vy-Vx)&&(Voltage_vector(2)==Vz) &&(theta_ac<120)
dip_vector=[0,1,0,0,1]; %type Gb
elseif (Vz<0.9*Vnom)&&(Vz-Vy > Vy-Vx)&&(Voltage_vector(3)==Vz) &&(theta_ab<120)
dip_vector=[1,1,0,0,1]; %type Gc

   %Unclassified dips
else dip_vector=[0,0,0,0,0];
end
```

```
function dip_name = ps_match_dip(D)
% matches the 5 element vector to the corresponding dip-type

dipmask=[0 1 0 1 0 1 0 1 0 1 0 1 0 1 0 1 0 1 0 1 ;
   0 0 1 1 0 0 1 1 0 0 1 1 0 0 1 1 0 0 1 1;
   0 0 0 0 1 1 1 1 0 0 0 0 1 1 1 1 0 0 0 0;
   0 0 0 0 0 0 0 0 1 1 1 1 1 1 1 1 0 0 0 0;
   0 0 0 0 0 0 0 0 0 0 0 0 0 0 0 0 1 1 1 1];

for i=1:20
   if D(:)-dipmask(:,i)==0;
      dip_type = i;
   switch dip_type
      case 1
         dip_name= 'NO MATCH FOUND';
      case 2
         dip_name='TYPE A';
      case 3
         dip_name= 'TYPE Ba';
      case 4
         dip_name='TYPE Bb';
      case 5
         dip_name='TYPE Bc';
      case 6
         dip_name='TYPE Ca';
      case 7
         dip_name='TYPE Cb';
      case 8
         dip_name='TYPE Cc';
      case 9
```

```
        dip_name='TYPE Da';
    case 10
        dip_name='TYPE Db';
    case 11
        dip_name='TYPE Dc';
    case 12
        dip_name='TYPE Ea';
    case 13
        dip_name='TYPE Eb';
    case 14
        dip_name='TYPE Ec';
    case 15
        dip_name='TYPE Fa';
    case 16
        dip_name='TYPE Fb';
    case 17
        dip_name='TYPE Fc';
    case 18
        dip_name='TYPE Ga';
    case 19
        dip_name='TYPE Gb';
    case 20
          dip_name='TYPE Gc';

  otherwise
    dip_name='ERROR SOMEWHERE';
end
  end
end
```

```
function x = show_class(dip_matrix)
% This function invokes ps_match_dip and create_dip_vector and uses the matrix
% dip_matrix

m=size(dip_matrix,1);
for i = 1:m
  show_type = lab_match_dip(lab_create_dip_vector(dip_matrix(i,:)));
  disp(show_type)
end
```

APPENDIX A-2 MATLAB™ FUNCTION CODE FOR BOLLEN CLASSIFICATION ALGORITHM (COURTESY OF DR M SCHILDER)

THE SIX-PHASE METHOD

```
function [t6,T6,V6,F6] = dipclsfy_six_1(va,vb,vc);

% SymDipClass  [t6,T6,V6,F6] = dipclsfy_six_1(va,vb,vc)
%
%                                   Function to classify dips using
%                                   6-Phase Method
%                                   Specific comparisons to SymDipClass
%
%                                   t6, T6 indicate type (and number) according to Bollen
classification
%                                   V6, F6 characteristic voltage and PNF
%                                   va,vb,vc are the complex phase voltages (single point data)

% Melanie Schilder
% 2004/11/15
% Copyright: Eskom R&S, CR&D
% rev3: 2006/05/15

% ------------------------------------ %
% Declare some useful constants                 %
% ------------------------------------ %
r2 = sqrt(2);
r3 = sqrt(3);
a = -1/2+j*r3/2;
a2 = a^2;
af = pi/180;

% ------------------------------------ %
% Calculate dip using 6-phase algorithm %
% ------------------------------------ %

  if abs(va)<eps, va = va+eps; end;
  if abs(vb)<eps, vb = vb+eps; end;
  if abs(vc)<eps, vc = vc+eps; end;

  vvec = [abs(va) abs(vb) abs(vc)];
  vrank = sort(vvec);
  vdiff = diff(vrank);


  v06 = (va+vb+vc)/3;

  va6 = va-v06;
  vb6 = vb-v06;
  vc6 = vc-v06;
  vab6 = (va-vb)/r3;
  vbc6 = (vb-vc)/r3;
  vca6 = (vc-va)/r3;

  Lvec = round(10000*[min((vbc6)) min((vc6)) min((vca6)) min((va6)) min((vab6)) min((vb6))])/10000;
  Mvec = round(10000*[max((vbc6)) max((vc6)) max((vca6)) max((va6)) max((vab6)) max((vb6))])/10000;

  T6 = find(abs(Lvec)==min(abs(Lvec)))-1;
  Fi = find(abs(Mvec)==max(abs(Mvec)))-1;
```

```
if length(T6)>1,
  if length(T6)==6,
    T6 = 6;
  else
    T6 = T6(1);
    Fi = Fi(1);
  end;
end;
if length(Fi)>1,
  Fi = Fi(1);
end;

if T6<6,
  V6 = Lvec(:,T6+1);
  F6 = Mvec(:,Fi+1);
else
  V6 = Lvec(:,1);
  F6 = Mvec(:,1);
end;

if (T6==0 & vdiff(1)<eps & vdiff(2)<eps),
  T6 = 6;
end;

if T6==0, t6 = 'Ca'; end;
if T6==1, t6 = 'Dc'; end;
if T6==2, t6 = 'Cb'; end;
if T6==3, t6 = 'Da'; end;
if T6==4, t6 = 'Cc'; end;
if T6==5, t6 = 'Db'; end;
if T6==6, t6 = 'A';  end;

B = (abs(vab6)^4+abs(vbc6)^4+abs(vca6)^4)./((abs(vab6)^2+abs(vbc6)^2+abs(vca6)^2)^2);
UB6 = sqrt((1-sqrt(3-6*B))/(1+sqrt(3-6*B)))*100;
if B>0.5,
  if B<0.5+eps,
    B = 0.5;
  else
    disp('Unbalance calculation error...(B>0.5)');
    %[ka kb kc pa pb pc]
    B-0.5
    UB6
  end;
end;
if B<1/3,
  if B<1/3-eps,
    B = 1/3;
  else
    disp('Unbalance calculation error...(B<1/3)');
    %[ka kb kc pa pb pc]
    B-1/3
    UB6
  end;
end;
```

THE SYMMETRICAL COMPONENT METHOD

```
function [ts,Ts,Vs,Fs] = dipclsfy_sym_1(va,vb,vc);

% SymDipClass  [ts,Ts,Vs,Fs] = dipclsfy_sym_1(va,vb,vc)
%
%                                   Function to classify dips using
%                                   Symmetrical Component Method
%                                   Specific comparisons to SixDipClass
%
%                                   ts, Ts indicate type (and number) according to Bollen
classification
%                                   Vs, Fs characteristic voltage and PNF
%                                   va,vb,vc are the complex phase voltages (single point data)

% Melanie Schilder
% 2004/11/15
% Copyright: Eskom R&S, CR&D
% rev3: 2006/05/15

% ------------------------------------ %
% Declare some useful constants                %
% ------------------------------------ %
r2 = sqrt(2);
r3 = sqrt(3);
a = -1/2+j*r3/2;
a2 = a^2;
af = pi/180;

% ------------------------------------ %
% Calculate dip using symmetrical components algorithm %
% ------------------------------------ %

  if abs(va)<eps, va = va+eps; end;
  if abs(vb)<eps, vb = vb+eps; end;
  if abs(vc)<eps, vc = vc+eps; end;

  vvec = [abs(va) abs(vb) abs(vc)];
  vrank = sort(vvec);
  vdiff = diff(vrank);

  A = [1 1 1; 1 a2 a; 1 a a2];
  Vseq = inv(A)*[va; vb; vc];
  v0s = Vseq(1);
  v1s = Vseq(2);
  v2s = Vseq(3);

  ks = (angle(v2s./(1-v1s))*180/pi+20)/60;
  %ks = (angle(v2s./(1-v1s))*180/pi)/60;
  Ts = round(ks);

  %UB = abs(v2s)./abs(v1s)*100;
  UB = abs(v2s./v1s)*100;
  if UB<eps,
    Ts = 6;
  end;

  if Ts~=6,
    while Ts>5,
```

```
    Ts = Ts-6;
  end;
  while Ts<0,
    Ts = Ts+6;
  end;
  if (Ts==0 & vdiff(1)<eps & vdiff(2)<eps),
    Ts = 6;
  end;
end;

V1 = v1s;
V2 = v2s;
V0 = v0s;

Vs = v1s-v2s*exp(-j*60*pi/180*(Ts));
Fs = v1s+v2s*exp(-j*60*pi/180*(Ts));

if Ts==0
  ts = 'Ca';
end;
if Ts==1
  ts = 'Dc';
end;
if Ts==2
  ts = 'Cb';
end;
if Ts==3
  ts = 'Da';
end;
if Ts==4
  ts = 'Cc';
end;
if Ts==5
  ts = 'Db';
end;
if Ts>=6
  ts = 'A';
end;

if length(Vs)>1
  [1 abs(va), abs(vb), abs(vc), angle(va)*180/pi, angle(vb)*180/pi, angle(vc)*180/pi, Vs, Fs]
end;
if length(Fs)>1
  [2 abs(va), abs(vb), abs(vc), angle(va)*180/pi, angle(vb)*180/pi, angle(vc)*180/pi, Vs, Fs]
end;

Vs = round(Vs*10000)/10000;
Fs = round(Fs*10000)/10000;
```

APPENDIX B-1: SIMULINK™ MODEL USED IN LABORATORY EXPERIMENT

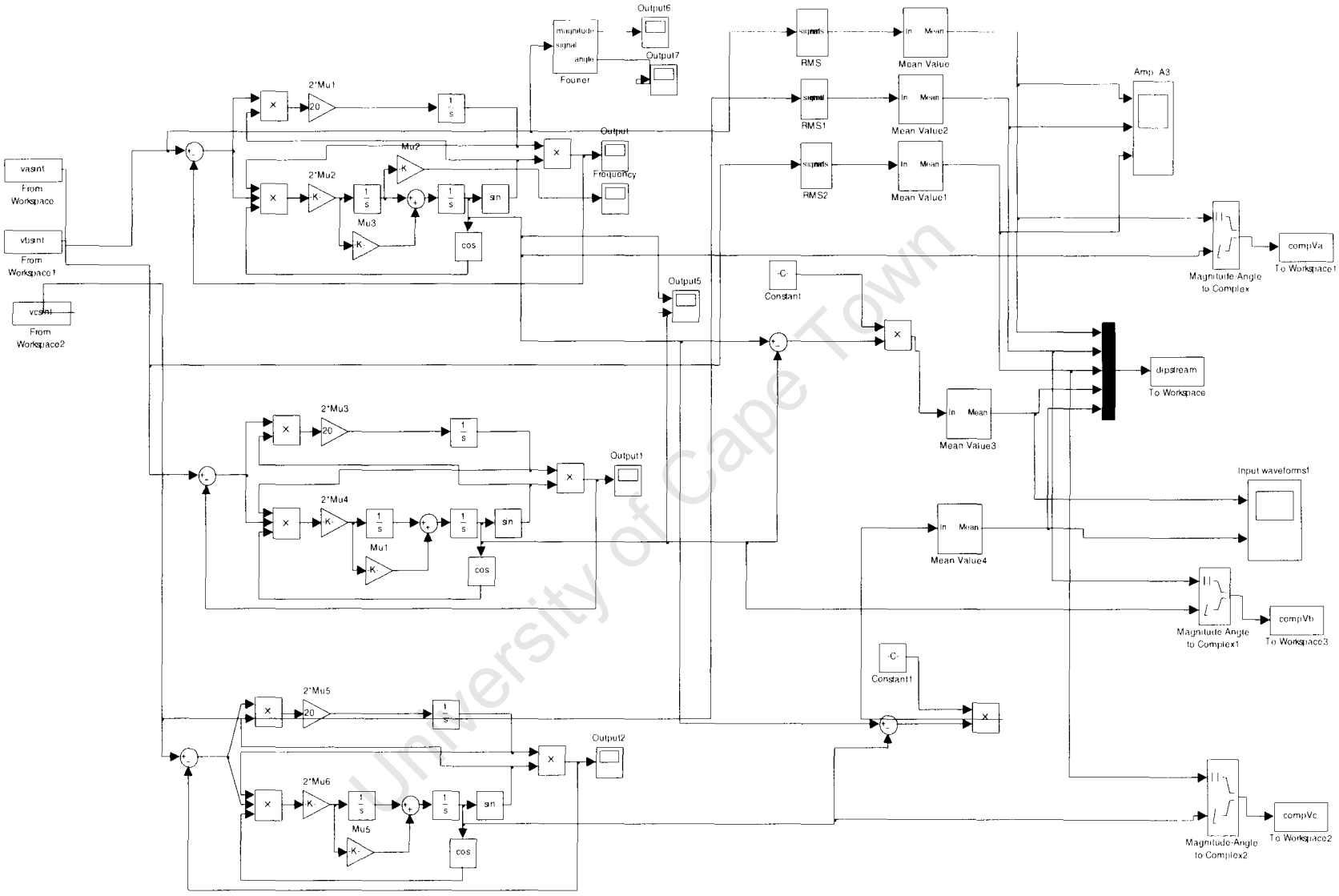

APPENDIX B-2: DIP GENERATOR SIMULINK™ MODEL